SPECTRAL INVESTIGATION OF SHOCKED PHYLLOSILICATES ON MARS USING CRISM AND THEMIS DATA

JOHANNA ERIKA S. VALDUEZA

July, 2016

SUPERVISORS:
MSc, W.H., Wim Bakker
Dr, H.M.A., Harald van der Werff

SPECTRAL INVESTIGATION OF SHOCKED PHYLLOSILICATES ON MARS USING CRISM AND THEMIS DATA

JOHANNA ERIKA S. VALDUEZA
Enschede, The Netherlands, July 2016

Thesis submitted to the Faculty of Geo-Information Science and Earth Observation of the University of Twente in partial fulfilment of the requirements for the degree of Master of Science in Geo-information Science and Earth Observation.
Specialization: Applied Earth Science

SUPERVISORS:
MSc, W.M, Wim Bakker
Dr, H.M.A., Harald van der Werff

THESIS ASSESSMENT BOARD:
Prof, Dr F.D., Freek van der Meer (Chair)
Prof, Dr S.M., Steven de Jong (External Examiner, Utrecht University)

ABSTRACT

From orbital near-infrared observations, numerous detections of phyllosilicates (clays) on Mars were commonly found in heavily cratered terrains, particularly in the southern hemisphere of the planet. These clays are believed to have formed during the Noachian era, the earliest time period on Mars when meteor bombardment was frequent in the solar system. In contrast, thermal-infrared orbital observations show less detection of clays in these areas.

Recent laboratory impact experiments of clay minerals could explain the spectral discrepancy between shortwave-infrared (SWIR) and thermal-infrared (TIR) wavelengths observed in Martian datasets. These experiments demonstrate that a damaged mineral structure by shock waves can cause spectral changes more apparent in TIR and less in SWIR. This is attributed to the fact that TIR is sensitive to the stretching and bending vibrations of silicon and oxygen bonds in the crystal structure while SWIR is sensitive to metal-OH and interlayer water. Moreover, impact effects in SWIR still retains diagnostic absorption features of a phyllosilicate despite affecting the hydration bands.

Therefore, this study utilizes CRISM and THEMIS data, currently the highest spatial and spectral resolution spectrometers showing the surface composition of Mars, to investigate impact/shock effects as possible cause of the spectral discrepancy. The SWIR and TIR spectral properties of phyllosilicates in different geologic contexts (crustal outcrop versus impact crater) were studied and compared in order to distinguish spectral properties of shocked phyllosilicates. The results of this analysis show that Fe/Mg phyllosilicates were identified both in SWIR and TIR wavelengths in different geologic contexts; however, the spectral discrepancy between the two wavelengths in phyllosilicate detection, particularly in the impact crater, can have multiple causes. Aside from impact/shock effects, limitations of summary products/spectral indices, presence of dusts, limited spatial resolution, and spectral mixing are among these causes.

Overall, direct evidence of the shocked phyllosilicate spectra in remotely sensed data cannot be obtained using the spatial and spectral resolution of the CRISM and THEMIS data. The results of this study may have implications on the detection of clay minerals in cratered terrains on Mars.

ACKNOWLEDGEMENTS

I would like to express my deepest gratitude to the following individuals and group of people who gave their time, effort, support, and guidance to help fulfill my dream of completing an MSc thesis related to Mars:

My supervisors, Mr Wim Bakker and Dr Harald van der Werff, for their advice, encouragement, and immediate feedback to improve this manuscript;

Dr Frank van Ruitenbeek for his inputs in this thesis during the proposal phase;

The ITC Faculty and the University of Twente for sponsoring my studies through the UTC-ITC Excellence Scholarship;

Mr Bart Krol for helping me apply for extension of studies and scholarship after missing a few months due to illness;

Dr Jennifer Piatek of Central Connecticut State University for patiently answering all my inquiries regarding jENVI software and THEMIS image processing;

Dr Gritters-van der Oever of Medische Spectrum Twente, for continuously monitoring my health for the past 8 months;

My 2014-2016 ITC Faculty batchmates, AES classmates, Filipino friends in Enschede, and ICF members for the fun and memories. Life in ITC is stressful; but whenever I'm with you guys, things are not as hard as they seem. Thank you also for all the prayers for my recovery. I would have not been able to reach this point without your prayers and support;

My family and my boyfriend, who took care of me and did everything to make sure I'll recover as soon as possible. Thank you so much for the love and sacrifice. You are my source of inspiration and motivation.

Greatest thanks to my God for all the love, grace, and blessings.

To God be the glory!

Ad Astra Per Aspera!

TABLE OF CONTENTS

LIST OF FIGURES

LIST OF TABLES

1. INTRODUCTION

Clays (phyllosilicates) on Earth evolved and resulted from chemical interactions between rock and water under certain environmental conditions, particularly changes in temperature and pressure, exposure or isolation to atmospheric conditions, and variations in water fluid chemistry and water availability (Hazen et al., 2013; Ehlmann et al., 2011). They are typically found at near surface environment and in hydrothermal systems (Meunier, 2005).

Through orbital observations, numerous detections of clays were also found on Mars. Spectral signatures of clay minerals were detected using near-infrared (NIR) to thermal infrared (TIR) wavelengths. The Observatoire pour la Minéralogie, l'Eau, les Glaces et l'Activité (OMEGA) spectrometer on board Mars Express (Bibring et al., 2005) at wavelengths 1.4, 1.9, and 3.0 μm has the capability to detect water absorption features which is indicative of hydrated sulfates and phyllosilicates in certain areas on Mars (Milliken et al., 2007). Two types of phyllosilicates were identified using OMEGA i.e. Fe/Mg-rich and Al-rich (Carter et al., 2013). Adding the hydrated minerals found by OMEGA, the use of Compact Reconnaissance Imaging Spectrometer for Mars (CRISM) on board the Mars Reconnaissance Orbiter, with higher spatial resolution (18 – 36m) and spectral wavelength range of 0.4 – 3.9 μm (Murchie et al., 2007), further confirmed the presence of phyllosilicates and sulfates. In addition, CRISM discovered other hydrated minerals such as carbonates, illite, muscovite, kaolinite, and zeolites (Ehlmann et al., 2009). Phyllosilicates were also detected at multi-spectral thermal-infrared (Viviano & Moersch, 2012) from 6.8 to 14.9 μm at 100-m spatial resolution of the Thermal Emission Imaging System (THEMIS) onboard Mars Odyssey (Christensen et al., 2004).

These detections of phyllosilicates were mostly restricted to old and heavily cratered terrains on Mars (Carter et al., 2013; Mustard et al., 2008). Crater count data and compositional stratigraphy of the clay minerals indicate a Noachian age (4.1-3.6 billion years ago) (Ehlmann et al., 2011) which coincides with the Late Heavy Bombardment period, where meteoritic impacts in the solar system were prevalent (Hazen et al., 2013). Since impact craters are considered as natural excavators, it is believed that the observed clay minerals were actually excavated materials from depth (Fairén et al., 2010) and formed under different conditions in the past since the present environmental conditions show a dry and cold Mars (Ehlmann et al., 2011).

However, when SWIR and TIR wavelengths were combined to give complementary information on the spectral properties of phyllosilicates on Mars, there was a spectral discrepancy observed between the two in the detection of phyllosilicates(Bandfield, 2002; McDowell & Hamilton, 2009; Michalski et al., 2010; Rogers & Bandfield, 2009). TIR detects less phyllosilicates compared to SWIR.

Recent laboratory impact experiments of phyllosilicates demonstrated that impact/shock effects could cause the spectral discrepancy (Che & Glotch, 2014; Friedlander et al., 2015; Gavin et al, 2013). These experiments showed that experimental impacts can alter the mineral structure, thus their spectra. SWIR is sensitive to the vibrations of metal OH and interlayer H_2O groups, while TIR is sensitive to the stretching and bending vibrations of silicon and oxygen bonds in the crystal structure (Michalski et al., 2010). Thus, damaged mineral structure due to impacts will be more apparent in TIR and less in SWIR.

Friendlander et al., 2015 laboratory experiments showed that the mineral structure of a Nontronite, most common clay mineral on Mars, becomes disordered when subjected to increasing shock/impact pressures. The SWIR is sensitive to the overtones of metal-OH in the nontronite octahedral sheets while the TIR is sensitive to the Si-O bending and stretching of the nontronite tetrahedral sheet (Friedlander et al., 2015). Their study has demonstrated that the tetrahedral and octahedral sheets deform differently causing the spectral difference between the SWIR and TIR. In SWIR, the nontronite can still be identified. However, the TIR spectra become amorphous with increasing shock pressure and can be observed in TIR region, specifically at 8-12 μm and 16-25 μm (Friedlander et al., 2015).

It was also confirmed that thermal effects from impacts can affect the SWIR spectra, resulting to reduced absorption depth of OH (dehydroxylation) and water (dehydration) absorption features, while still retaining characteristic spectral features of a phyllosilicate (Che & Glotch, 2012, 2014). These laboratory impact studies support that phyllosilicates associated with impact craters were previously existing materials and were exposed to metamorphism due to meteor impacts.

In this thesis, I will examine the SWIR and TIR spectral properties of phyllosilicates associated with impact craters in the Tyrrhena Terra region on Mars, using CRISM and THEMIS data. This is one of the heavily cratered regions where researchers, using OMEGA and CRISM, have detected a presence of clay minerals. Moreover, the phyllosilicates in this area were considered to be directly related to impact processes – either were excavated from depth by impacts and were already pre-existing materials formed by subsurface hydrothermal processes or were altered due to shock metamorphism from impacts (Loizeau et al., 2012). This is different from other regions such as Nili Fossae where near surface weathering processes are considered to be responsible for the presence of phyllosilicates and impact cratering only played a minor role (Loizeau et al., 2012). Thus, in order to assess whether the spectral properties of phyllosilicates associated with impact craters are distinct in remotely sensed data, a spectral comparison between phyllosilicates in the crustal outcrop in Nili Fossae and phyllosilicates in an impact crater in Tyrrhena Terra was carried out. The result of this comparison is expected to provide insights on spectral differences in the SWIR and TIR datasets observed in previous studies. This also validates the results from laboratory experiments which showed impact/shock effects could cause the spectral discrepancy.

1.1. Study Region

Tyrrhena Terra is located in the elevated areas of the southern hemisphere on Mars (Fig. 1). This region is composed of Noachian-aged (4.1-3.7 billion years ago) craters with a few scattered Late Noachian (3.6-3.8 billion years ago) - Hesperian (3.5-2.9 billion years ago) units and is bounded by Isidis Planitia and Syrtis Major volcano to the North, Hesperia Planum to the east, and Hellas basin to the south (Loizeau et al., 2012). Although the study area is dissected by outflow channels, most of the impact craters are well-preserved and are not eroded by fluvial activity (Loizeau et al., 2012).

The phyllosilicates observed in Tyrrhena Terra are possibly directly related to impact processes; which makes it different from areas such as Nili Fossae, a group of concentric grabens or crustal fractures, where phyllosilicates are mostly result of shallow to near surface alteration processes rather than impact processes (Loizeau et al., 2012). Therefore, the Tyrrhena Terra region seems suitable to study the spectral properties of phyllosilicates in impact craters, and distinguish this from the spectral properties of phyllosilicates which are not directly the result of impacts such as in Nili Fossae.

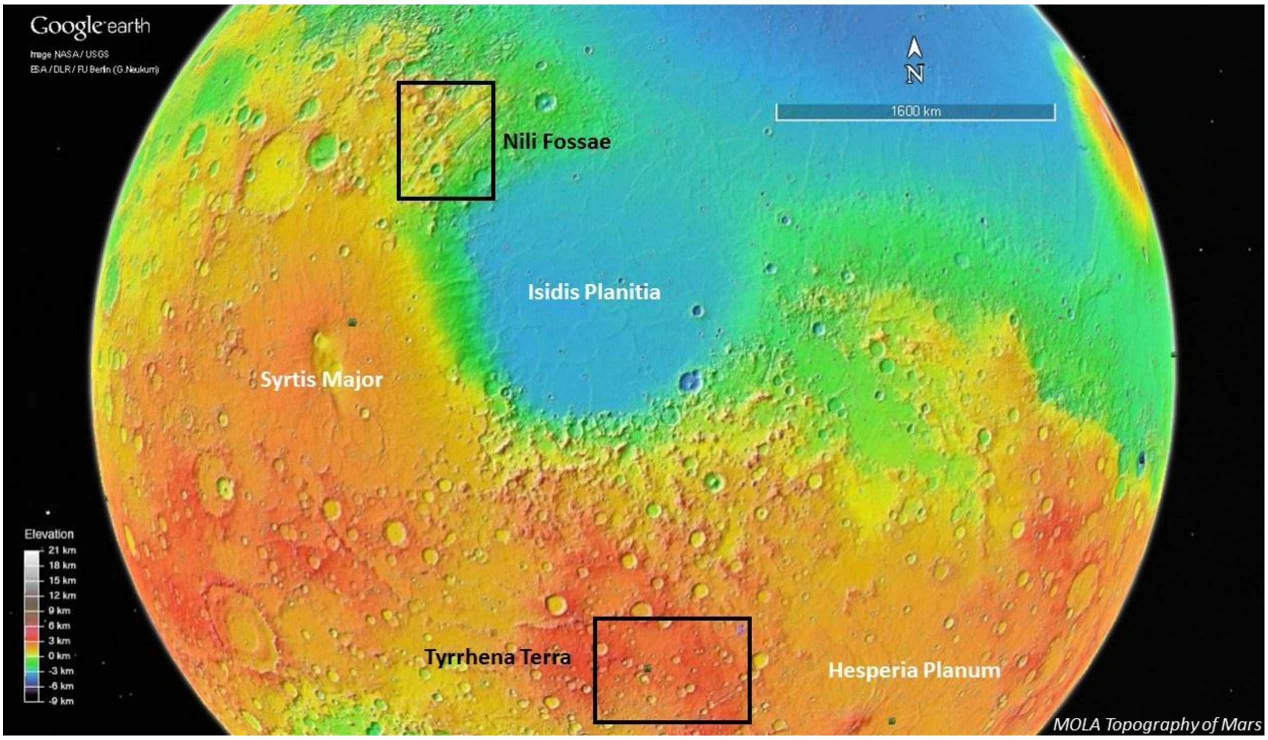

Figure 1: MOLA (Mars Orbital Laser Altimeter) topography of Mars in Google Earth. Black boxes show study areas.

1.2. Research Objectives and Questions

The main objective of this thesis is to characterize spectral properties of phyllosilicates associated with impact craters using hyperspectral CRISM SWIR and multispectral THEMIS TIR data.

The specific objectives are the following:

- To examine the near-infrared and thermal infrared spectra of phyllosilicates associated with impact craters
- To distinguish the spectral properties of a shocked phyllosilicate that are possibly caused by impact processes

Research questions that arise from the above objectives are:

- Can CRISM and THEMIS complement each other in order to identify phyllosilicates?
- What are the challenges in combining CRISM and THEMIS data?
- What can we conclude from comparing the spectral properties of phyllosilicates from impact craters with those that are not related to such geologic features?
- What would be the similarities or differences of the spectral changes observed from laboratory experiments with that of remotely sensed data and what are the possible conditions that could cause these differences?

2. METHODS

Figure 2 provides an overview of the methodology, data processing, spectral analysis, and the outputs. These methods aim to answer the first three research questions presented in Chapter 1. The last research question will be dependent on the results of the previous questions and will be further discussed in Chapter 4.

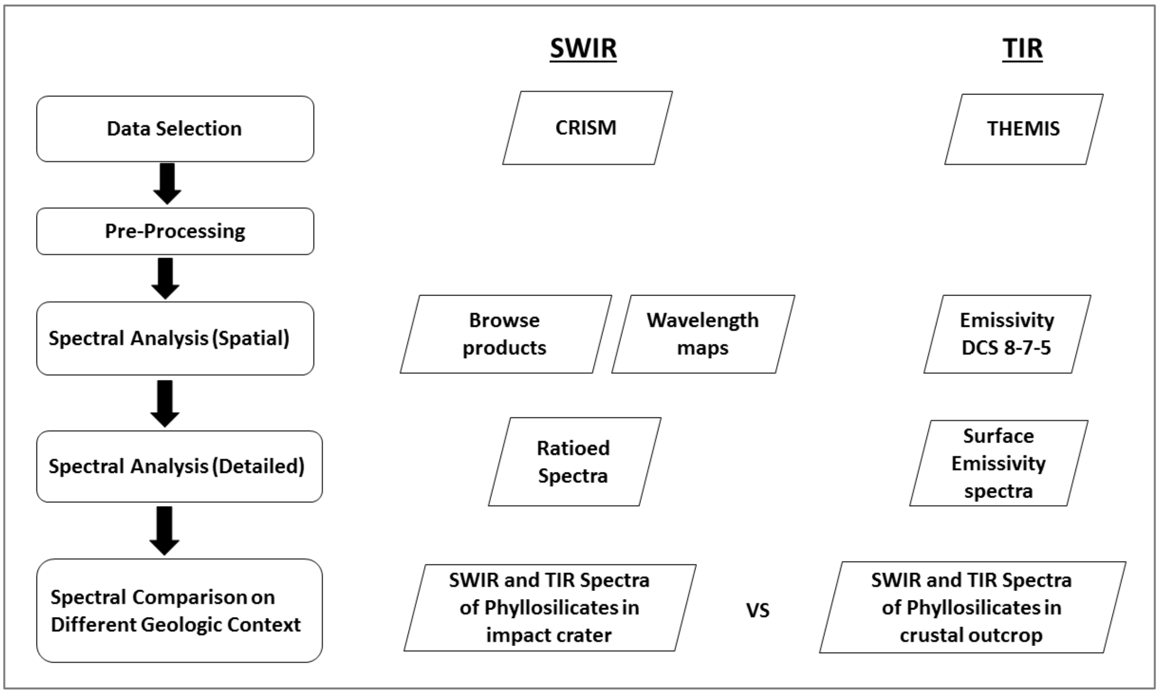

Figure 2: Overview of Methodology

2.1. CRISM and THEMIS datasets

In this study, I took advantage of the high spatial resolution and spectral range of CRISM and THEMIS spectrometers to resolve the spectral properties phyllosilicates in different geologic context. The main characteristics of these instruments are shown in Table 1. For CRISM, I only used the full-resolution targeted data (FRT) and selected a spectral range of 1.0 to 2.7 μm, in which diagnostic vibration absorption features of H_2O and OH in phyllosilicates are observed. I used the daytime thermal infrared data from THEMIS to acquire the surface emissivity spectra for the spectral analysis.

Instrument name	Mapping/Survey Mode	Spatial Resolution	Spectral Range
CRISM (Compact Reconnaissance Imaging Spectrometer for Mars)	Hyperspectral Targeted: Full-resolution (FRT) Half-resolution (HRT) Multispectral	 18 m 36 m 100 or 200 m	0.362 - 3.920 μm (544 bands) (72 bands)
THEMIS (Thermal Emission Imaging System)	Visible/Near-infrared multispectral: Thermal Infrared multispectral: Daytime Nighttime	100 m	0.42 – 0.86 μm (5 bands) 6.8 – 14.9 μm (9 bands) 12.57 μm (1 band)

Table 1: Characteristics of CRISM and THEMIS spectrometers

2.2 Data Selection

Images were selected based on availability and coverage. I implemented this step in Google Mars and JMARS (Christensen et al., 2009); both are open access data visualization and GIS software where various datasets were accessed, combined, and overlaid for rapid assessment.

These are the selection criteria:

- The impact crater should be well-preserved where its parts such as crater peak, wall, floor, rim, and ejecta are evident. It should also be >7km in diameter. The crater size is related to the depth of the excavation by impact and the >7km size shows that the impact was deep enough to reach the phyllosilicates assumed to be pre-existing in the subsurface (Barnhart & Nimmo, 2011).

- CRISM full-resolution targeted (FRT) data are available for the chosen impact crater and crustal outcrop. The available data for the impact crater should cover all impact features mentioned above.

- CRISM summary products based on multispectral parameters by Pelkey et al. (2007) are available. These products can be used to quickly check the presence and relative abundance of clay minerals in the crater before spectral analysis using hyperspectral data. Preference is for craters that show strong (i.e. high relative abundance) NIR spectral signature of phyllosilicates.

- THEMIS daytime infrared images are available for that crater and have certain parameters that should be noted for this study. Images should have average surface temperatures of ≥240 K and low average atmospheric dust and water opacities (≤ 0.15) (Viviano & Moersch, 2013). Using these factors increases the signal-to-noise ratios in the scenes. (Baldridge et al., 2013; Viviano and Moersch, 2013). This initial inspection of THEMIS datasets will be performed in JMARS.

2.3 Data Processing and Spectral Analysis

2.3.1. CRISM Data Processing

Considering the selection criteria, images were selected and downloaded from NASA's Planetary Data System (PDS) Geosciences Node website (http://ode.rsl.wustl.edu/mars/). These images were processed in ENVI version 5.1 using CRISM Analysis Toolkit (CAT) version 7.3.1 (Morgan et al., 2009). CAT is an ENVI plugin developed for CRISM data processing to correct for the viewing geometry and atmospheric effects of the CRISM images. This tool is also available from the PDS website.

The downloaded CRISM images from PDS were already converted to apparent I/F (the ratio of reflected to incident sunlight) using procedures described by Murchie et al., 2007 which involve three steps. The detector background is initially removed from the CRISM data by using systematic measurements of the dark current that are included in Mars scene measurements. The data is then calibrated to radiance by dividing measurements of radiance emitted by an onboard integrating sphere and then multiplied by a spectral model of the integrating sphere derived from ground calibrations. Lastly, the apparent I/F is generated from the calibrated radiance data by dividing it by a solar spectrum. This solar spectrum is convolved to the CRISM's wavelengths and resolution measured on the ground and scaled to Mars' solar distance.

The CRISM images are in PDS format. To proceed with the viewing geometry and atmospheric corrections using CAT, the images were first converted to CAT format (Fig. 3). The photometric correction was used to correct for the illumination geometry; where the CRISM I/F data is divided by the cosine of the solar incidence angle (Murchie et al., 2007). The Martian atmosphere is composed of 95% CO_2 (Owen et al., 1977), which produces deep and narrow absorptions bands, notably between 1.9-2.1 μm (Martin & Barker, 1932). This interferes with the detection of hydration bands at the same wavelengths. To suppress the atmospheric effects, I used the volcano-scan technique by McGuire et al. (2009) which divides each observed spectrum by the atmospheric transmission spectrum derived from observations at the base and top of Mount Olympus on a Martian day when the amounts of ice and dust aerosols were minimal.

2.3.2. CRISM Summary Products and Wavelength Mapping

Following the pre-processing, the CRISM summary products/spectral parameters were generated from each images and map-projected (Fig. 3). The summary products are designed and formulated to capture spectral features unique to a specific mineralogy (Pelkey et al., 2007). The spectral parameters were then combined to form a color composite or called browse product, which detects various types of minerals (Viviano-Beck et al., 2014). This study looks for the presence of phyllosilicates, and takes advantage of color composites of summary products to identify such mineralogy in the impact crater and in the crustal outcrop. Although it was mentioned in Section 2.2 that summary products by Pelkey et al. (2007) were used for quick assessment of the images, the summary products shown in Fig. 3 are generated based on the expanded parameter set by Viviano-Beck et al.(2014) that exploits CRISM's hyperspectral data.

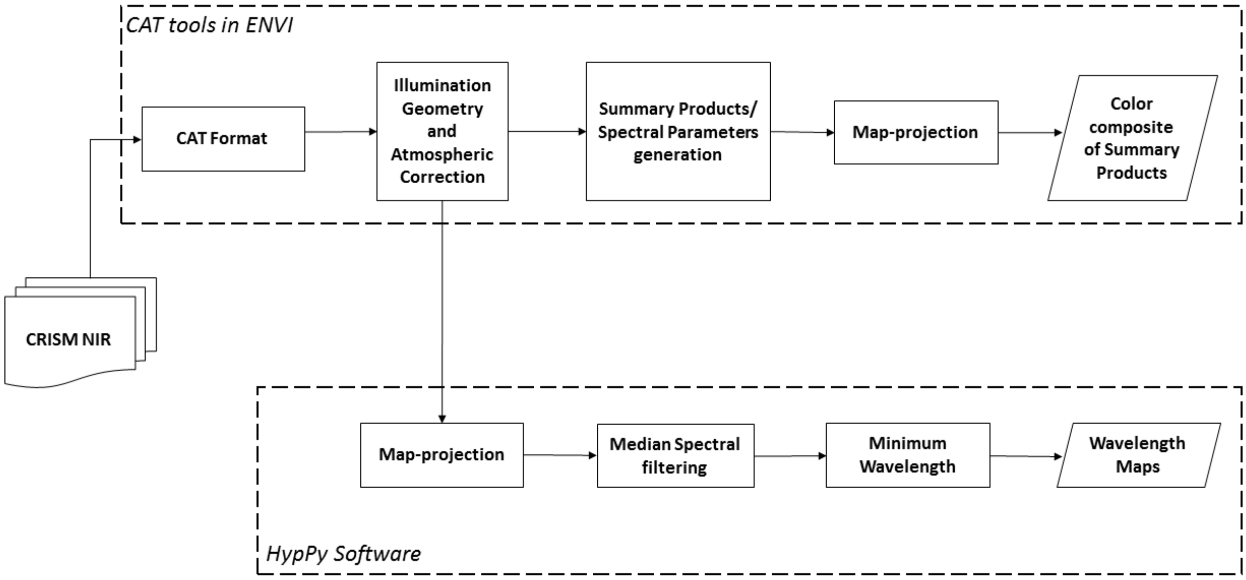

Figure 3: Workflow for CRISM data. Dashed boxes show what software was used to perform the processing.

Wavelength maps were generated for each image and used to complement the CRISM summary products. Wavelength mapping is a pre-classification technique which identifies the wavelength position and depth of the deepest absorption features between 2.1 and 2.4 μm, a spectral range where hydrous minerals such as phyllosilicates contain diagnostic absorption features (van Ruitenbeek et al., 2014). In a wavelength map, the wavelength position of the deepest absorption feature is represented in color and its depth in intensity (van Ruitenbeek et al., 2014). In this study, prior to applying wavelength mapping, median spectral filtering was applied to the atmospheric-corrected CRISM images to filter systematic and random noise in the data (Bakker et al., 2014). The wavelengths of the deepest absorption features were then identified in order to generate the wavelength maps. The procedure for wavelength mapping was performed in HypPy software developed by Bakker (2013).

2.3.3. CRISM Detailed Spectral Analysis

Spatially distinct patterns observed from the summary products and wavelength maps were used in choosing regions of interest (ROIs) in the crater and in the crustal outcrop. This step focuses on enhancing phyllosilicate absorption features, therefore the spectral identification of a spatial region lacking absorption features are not taken into account in this study. An average spectrum was extracted per ROI (Table A1). This average spectrum was ratioed to a nearby ROI with an average spectrum that lacks narrow absorption features located in the same image column (Parente, 2008). This method is called spectral ratio. In ENVI, a spectral ratio was performed by choosing the target spectrum as the numerator and the spectrum that lacks narrow absorption feature as the denominator. This spectral ratio reduces cross-image artefacts, systematic noise, and remaining atmospheric effects in the data, eventually enhancing the absorption features (Ehlmann et al., 2009). The resulting spectra were compared to the CRISM spectral library (Vivian-Beck et al., 2015) which I included in CAT for mineral identification.

2.3.4. THEMIS Data Processing

THEMIS daytime infrared images were chosen according to Section 2.2 and were downloaded from the THEMIS website (http://themis-data.asu.edu/). THMPROC (http://thmproc.mars.asu.edu/), an online site for simplifying THEMIS processing for users, was used to correct for viewing geometry, projection, and removal of atmospheric emission. These pre-processing methods for THEMIS were adapted from Bandfield et al.(2004).

Radiance images were acquired using the standard processing of THEMIS IR data in THMRPOC, which include undrift/dewobble (UDDW) filter, rectify, deplaid filter, auto-radcorr (Automatic radiance correction), and unrectify (Fig. 4). All these procedures are for systematic and noise corrections in the THEMIS IR data (Murray et al., 2012). The UDDW filter removes data variations due to temperature changes in the IR detector array. The Rectify algorithm eliminates most of the black stripes present in a projected THEMIS IR data. The deplaid filter is used to remove line and row correlated noise in a rectified THEMIS IR image. The auto-radcorr technique removes the radiance from atmospheric emission with no user input required and eliminates elevation effects in the THEMIS radiance data. Lastly, the Unrectify algorithm brings back the original projection of the THEMIS IR radiance data and is necessary for ENVI to read the file.

jENVI, a THEMIS processing tool in ENVI developed by Piatek and Moersch (2006), was used to further process the THEMIS IR radiance data to extract apparent emissivity (Fig. 4). Similar with THMRPOC, the THEMIS processing methods in jENVI were also adapted from Bandfield et al. (2004). Using the 'Process THEMIS' routine in jENVI, the THEMIS IR radiance data was separated into temperature and emissivity using a normalized emissivity method (with an assumed emissivity of 1.0). The normalized method calculates temperature using the assumed emissivity and radiance in each band and selects the highest value of temperature in each pixel as the surface temperature for the temperature/emissivity separation (Gillespie, 1986).

The apparent emissivity consists of surface and non-surface components such as atmospheric effects (Tornabene et al., 2008). To derive the corrected surface emissivity, a TES Bootstrap correction was applied (Bandfield et al., 2004). In this method, the atmospheric-corrected surface emissivity spectra retrieved from TES (Thermal Emission Spectrometer) data, a hyperspectral thermal infrared imager with a courser spatial resolution than THEMIS (Christensen et al., 2001), was used to determine atmospheric contributions for a selected area of a THEMIS image (Bandfield et al., 2004). This is performed by choosing an ROI in the THEMIS image that is spectrally uniform and forcing its average spectrum to match a TES atmospheric-corrected emissivity spectrum that overlaps that area in the THEMIS image to do the correction. TES data were obtained from JMARS.

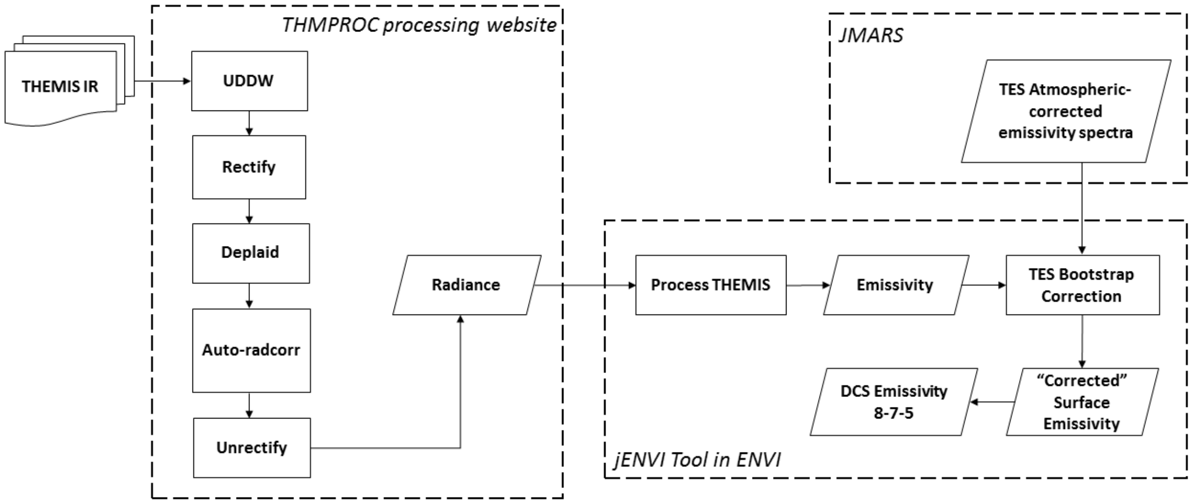

Figure 4: Workflow for THEMIS data. Dashed boxes show what software was used to perform the processing.

2.3.5. THEMIS Decorrelation Stretch and Detailed Spectral Analysis

A decorrelation stretch (DCS) was applied to the atmospheric-corrected surface emissivity data to maximize spectral variations among bands of the THEMIS image (Gillespie et al., 1986). Bands 8, 7, and 5 were used for the DCS (see Table 2 for wavelengths). In a DCS 8-7-5 image, shorter wavelength absorptions appear yellow and reveal the presence of phyllosilicates or minerals with higher silica content, while longer wavelength absorptions appear purple, red, and cyan and indicate the presence of mafic minerals (Amador & Bandfield, 2016; Baldridge et al., 2013; McDowell & Hamilton, 2009; Salisbury & Walter, 1989). The averaged emissivity spectrum from an ROI was extracted in an area that indicates presence of phyllosilicates as identified from the CRISM images (Table A1).

Band	Wavelength (μm)
1	6.78
2	6.78
3	7.93
4	8.56
5	9.35
6	10.21
7	11.04
8	11.79
9	12.57
10	14.88

Table 2: THEMIS IR spectral bands

2.4 Spectral Comparison in Different Geologic Context

In order to distinguish the shortwave-infrared (SWIR) and thermal-infrared (TIR) spectral properties of a shocked phyllosilicate, a comparison was made between the spectra of phyllosilicates in crustal outcrop in Nili Fossae and the impact crater in Tyrrhena Terra. The Nili Fossae area is believed to be less altered by impact processes and any phyllosilicates can thus be considered as non-shocked. Results from the SWIR and TIR (spatial) spectral analysis (e.g. browse products and wavelength maps) in both geologic contexts were draped on Google Mars for visual analysis. The extracted SWIR and TIR spectra of phyllosilicates from two different geologic context were studied by looking at characteristic absorption features that may indicate possible impact effects as described in laboratory impact experiments. This approach is illustrated in the next chapter.

This chapter has described in detail the criteria used in selecting datasets for spectral analysis, and the different techniques applied to extract the ratioed spectra of phyllosilicates from CRISM SWIR and the surface emissivity spectra of phyllosilicates from THEMIS TIR. The outputs were compared based on the spectral detection of phyllosilicates in different geologic context to distinguish the spectral properties of a shocked phyllosilicate (Fig. 2). All these methods aim to answer the first three research questions. The spectral comparison in different geologic contexts is illustrated in the following chapter.

3 RESULTS

The results are divided into spectral detection of phyllosilicates in a different geologic context: the Tyrrhena Terra impact crater and the Nili Fossae crustal outcrop. Each division contains the results from data selection, and spatial and detailed spectral analyses of the differences between SWIR and TIR in phyllosilicate detection.

3.1 Tyrrhena Terra Impact Crater

3.1.2. Selected Data

As observed from Google Mars, most impact craters in the Tyrrhena Terra region are not completely covered by the CRISM FRT data and the multispectral summary products. In many cases, only certain parts such as crater peak or a section of a crater rim were covered. In JMARS, THEMIS IR data show a large coverage of impact craters in Tyrrhena Terra. However, very few of these images meet the data selection criteria, where average surface temperature should be ≥ 240 K and low amount of atmospheric dust and water opacity ≤ 0.15.

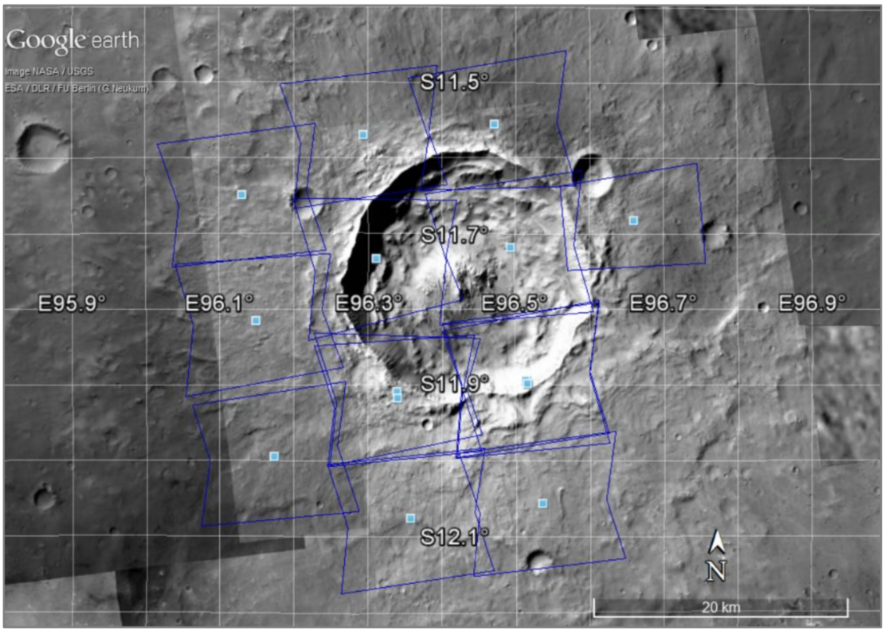

Figure 5: Selected unnamed impact crater in Tyrrhena Terra. Blue boxes show CRISM data coverage. All are CRISM FRT data, except for the rightmost blue box which is an HRT (half-resolution targeted) data.

Based on the selection criteria presented in Section 2.2, only one impact crater (-11.753° S, 96.476° E) in Tyrrhena Terra met the requirements. This unnamed impact crater has a diameter of approximately 19km and shows a well-preserved crater peak, rim, floor, and ejecta. There are 11 CRISM FRT images covering different parts of the crater and its corresponding multispectral summary products show the presence of phyllosilicates. Only one THEMIS image was selected which only covers the eastern section of the impact crater. This image has an average surface temperature of 252.70 K and an average amount of atmospheric dust and water opacity of 0.15. Table 3 shows the Image ID of the CRISM and THEMIS datasets used.

Datasets	Image ID
CRISM FRT	frt0001652d_07_if164l_trr3 frt0000b291_07_if164l_trr3 frt00006483_07_if164l_trr3 frt00013e2f_07_if164l_trr3 frt000188f8_07_if164l_trr3 frt00013844_07_if164l_trr3 frt0000cb68_07_if164l_trr3 frt0000881f_07_if164l_trr3 frt00007b2b_07_if164l_trr3 frt000060b2_07_if164l_trr3 frt00008ef8_07_if164l_trr3
THEMIS Daytime IR	I17695028

Table 3: CRISM and THEMIS datasets used for the Tyrrhena Terra impact crater (-11.753° S, 96.476° E) study.

3.1.2. CRISM NIR Summary Products and Wavelength Maps

Several browse products, which are color composites of summary products/spectral parameters, were generated using CAT to detect a possible presence of hydrous minerals in the crater (Table 4). These browse products were derived from Viviano-Beck et al. (2014). Among these browse products, only the Fe/Mg phyllosilicates (PFM) browse product, a combination of summary products BD2355, D2300, and BD2290, displayed a spatially distinct pattern of hydrous minerals in the impact crater, particularly Fe/Mg phyllosilicates, which consists of two distinct colors - cyan and yellow (Fig. 6A). A cyan color exhibits more presence of both D2300 and BD2290 summary products than BD2355; while a yellow color displays more presence of BD2355 and D2300 than BD2290. This means that the cyan color indicates a presence of Fe/Mg smectites, while yellow can indicate a presence of chlorite, prehnite and epidote (Viviano-Beck et al., 2014).

Browse Product	Summary Products/Spectral Parameters
PHY (Phyllosilicates)	R: D2300, G: D2200, B: BD1900r2
PFM (Iron/Magnesium Phyllosilicates)	R: BD2355, G: D2300, B: BD2290
PAL (Aluminum Phyllosilicates)	R: BD2210_2, G: BD2190, B: BD2165
HYS (Hydrated Silica)	R: MIN2250, G: BD2250, B: BD1900r2
CAR (Carbonates)	R: D2300, G: BD2500_2, B: BD1900_2

Table 4: Browse products and their respective summary products/spectral parameters to check for hydrous minerals

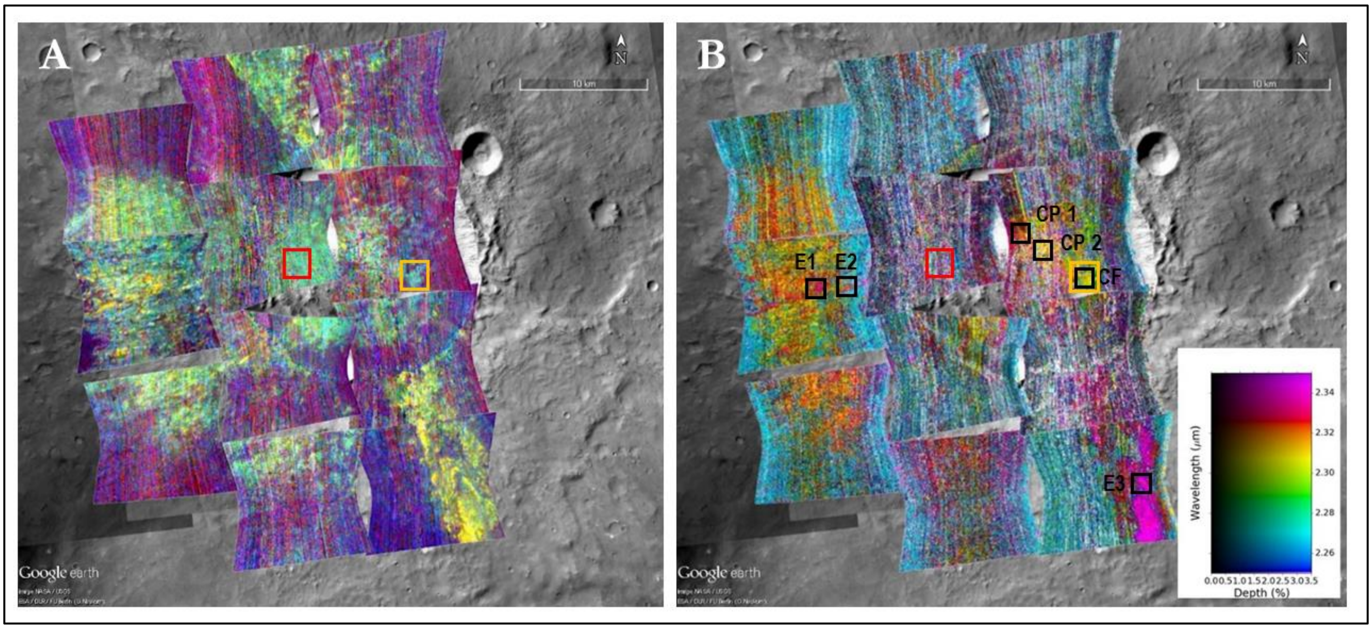

Figure 6: PFM browse products (A) and Wavelength maps (B) for the impact crater. Average spectra were extracted based on the combined results. CP 1 – Crater Peak 1, CP 2 – Crater Peak 2, CF – Crater Floor, E1 – Ejecta 1, E2 – Ejecta 2, and E3 – Ejecta 3.

Wavelength maps showed the occurrence of the deepest absorption features between 2.25 and 2.35 μm (Fig. 6B). The depth of the absorption features reaches up to 3.5% (Fig. 6B). Notably, these maps provided additional information to the distinct patterns and colors observed from the PFM browse products. For example, the area having a yellow color in the PFM browse product shows absorption features between 2.33 and 2.34 μm in the wavelength map. Moreover, the area with a cyan color in the PFM browse product appears to contain spectral mixtures in the wavelength map – one spectrum that is lacking diagnostic absorption features of a Fe/Mg phyllosilicate (see red boxes in Fig. 6) and the other spectrum which contains Fe/Mg phyllosilicates absorption features at 2.30 and 2.31 μm (see yellow boxes in Fig. 6).

3.1.3. CRISM NIR Spectral Ratio

The combined results from the PFM browse products and wavelength maps served as a guide to locate and extract representative regions of interest in the impact crater (Fig. 6B, Table A1). The average spectra of these regions were then enhanced using the spectral ratio method mentioned in section 2.3.3. Since the cyan color in the PFM browse product was found to contain mixtures of spectra, the region having a spectrum that lacks diagnostic absorption features of a phyllosilicate was used as denominator (described in section 2.3.3.) in the spectral ratio method to improve the absorption features of the phyllosilicate spectra being studied.

The unratioed and ratioed average spectra of the Fe/Mg phyllosilicates extracted in the crater peak, crater floor, and ejecta are shown in Figures 7 and 8.

In general, the ratioed average spectra in different parts of the crater display absorption features in ~1.4μm, ~1.9μm, and between 2.30 and 2.35 μm (Fig. 7 and 8). The ~1.4 μm and ~1.9 μm absorption features are caused by hydration bands such as hydroxyl and water whereas features between 2.30 and 2.35 μm are due to Fe/Mg-OH bonds (Bishop et. al, 2008). These absorptions were only found in the crater peak, crater floor, and ejecta. No features were found in the crater wall and rim. Crater Peak 1 (CP1) and Crater Floor (CF) also have features at 2.25 μm due to the absorption of the Al-OH bond. However, Crater Peak 2 (CP2) lacks the 2.25 μm feature while the CF lacks the 1.9 μm feature. Ejecta 1 (E1) has a dominant 1.9 μm feature, unlike Ejecta 2 (E2) and Ejecta 3 (E3) which do not have the 1.9 μm feature. The ~1.4μm absorption feature is found to be very subtle in all spectra.

When compared to the CRISM NIR spectral library, the spectrum of chlorite resembled the observed spectra (Figures 7 and 8) in the impact crater because of narrow absorptions features at 2.3-2.35 μm; except for E1 which is possibly a Fe/Mg smectite because of the strong 1.9 μm absorption feature not dominant in a chlorite spectra.

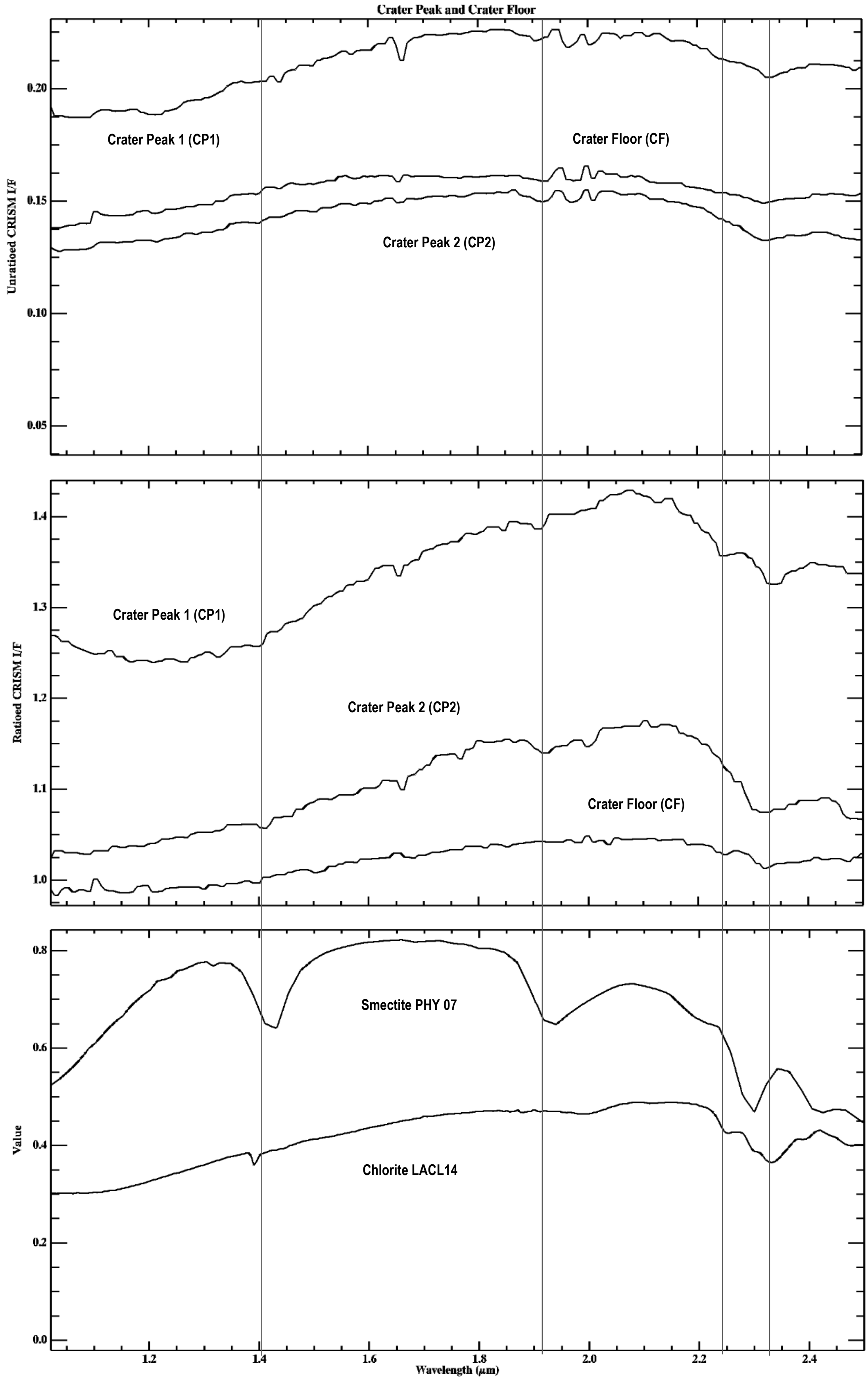

Figure 7: Unratioed and Ratioed average spectra from the crater peak and floor. Gray lines show diagnostic absorption features of Fe/Mg phyllosilicate. CRISM library spectra are shown for comparison.

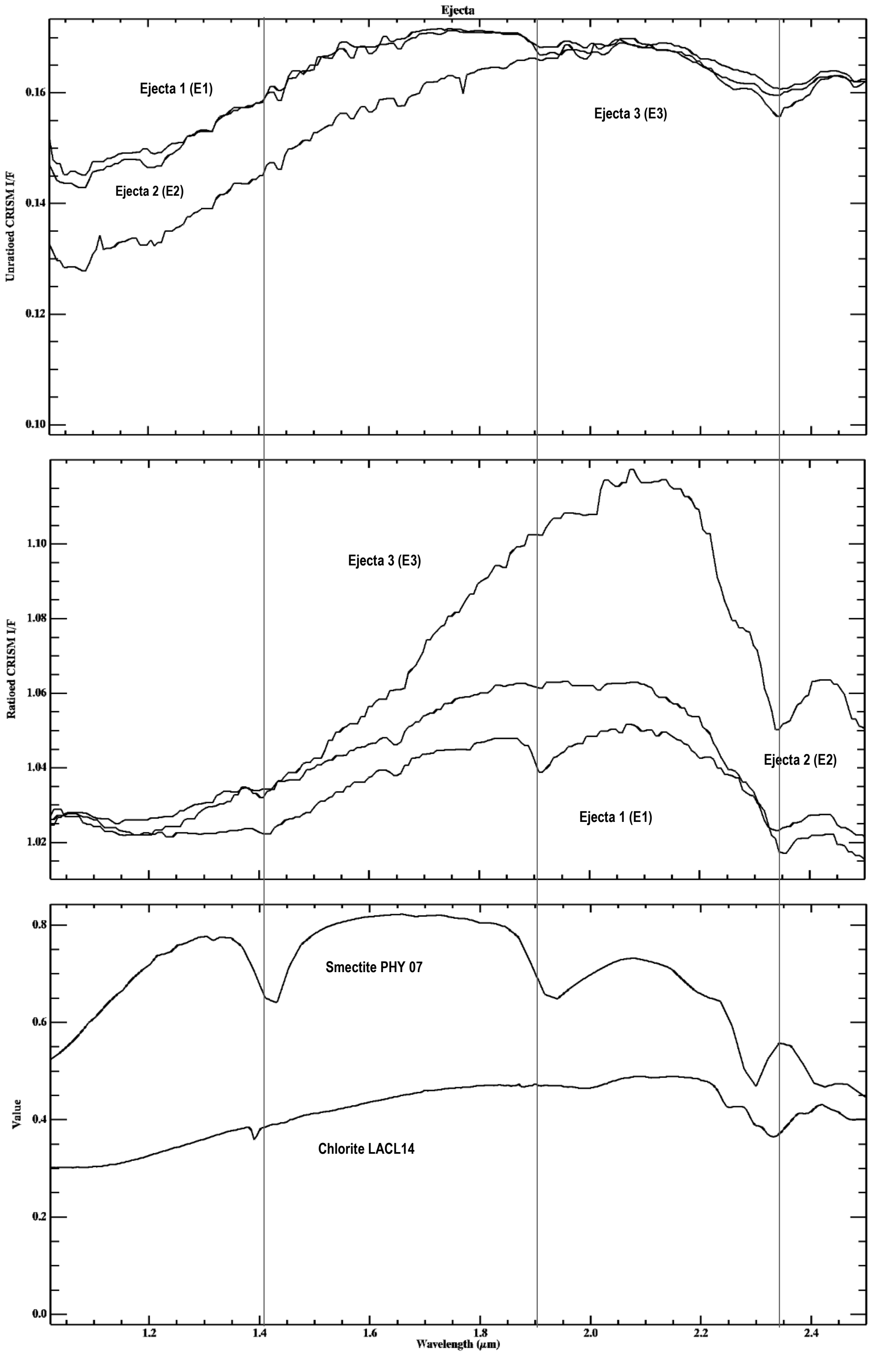

Figure 8: Unratioed and Ratioed average spectra from the ejecta. Gray lines show diagnostic absorption features of Fe/Mg phyllosilicate. CRISM library spectra are shown for comparison.

3.1.4 THEMIS TIR Decorrelation Stretch and Surface Emissivity Spectra

The DCS emissivity 8-7-5 (described in section 2.3.5) image displayed spectral variations in five components: magenta/purple, red, cyan, yellow, and green. Magenta is mainly found in the crater peak and surrounding plains, red in the plains, yellow in the crater floor and ejecta, cyan mostly in the crater rim, and green in the ejecta (Fig. 9).

Since this study aims to look at thermal-infrared spectra for shocked phyllosilicates, the selected ROIs with average surface emissivity spectra (Table A1) should also overlap with the ROIs from the CRISM SWIR data that were identified as Fe/Mg phyllosilicates.

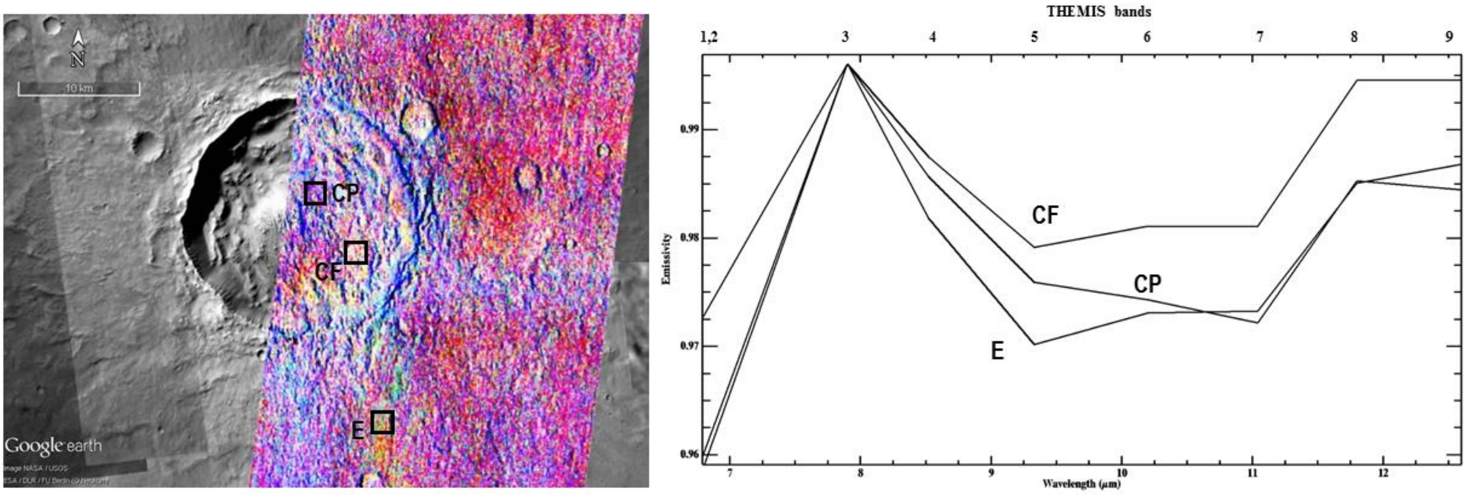

Figure 9: THEMIS DCS 8-7-5 emissivity image of the Tyrrhena Terra impact crater (Left image). Average emissivity spectra extracted from ROIs in the emissivity image (Right image). CP - Crater Peak, CF - Crater Floor, and E – Ejecta.

In general, the emissivity spectrum from each ROI (Fig. 9) appears to contain spectral mixtures because of the two prominent emissivity lows visible in bands 5 and 7. The emissivity low in band 5 matches with the TIR spectra of Fe/Mg phyllosilicates in the TIR spectral library (http://speclib.asu.edu/), which have emissivity lows between bands 5 and 6. The emissivity low in band 7 matches with the TIR spectra of Olivine in the spectral library which has emissivity low in band 7 (Fig. 10).

The ROI in the crater peak (CP) appears similar to the surrounding plains because of its magenta/purple color in DCS 8-7-5 (Fig. 9). Comparing its emissivity in band 5 and band 7, the latter has a lower emissivity which could imply a higher relative abundance of olivine than Fe/Mg phyllosilicate. On the other hand, the ROIs in the crater floor (CF) and in the ejecta (E) have similar spectral character, but the latter has a lower emissivity in bands 5 and 7. Moreover, the emissivity of CF and E in band 5 is lower than band 7, hence the crater floor and the ejecta of the impact crater contain higher relative abundance of Fe/Mg phyllosilicates than olivine.

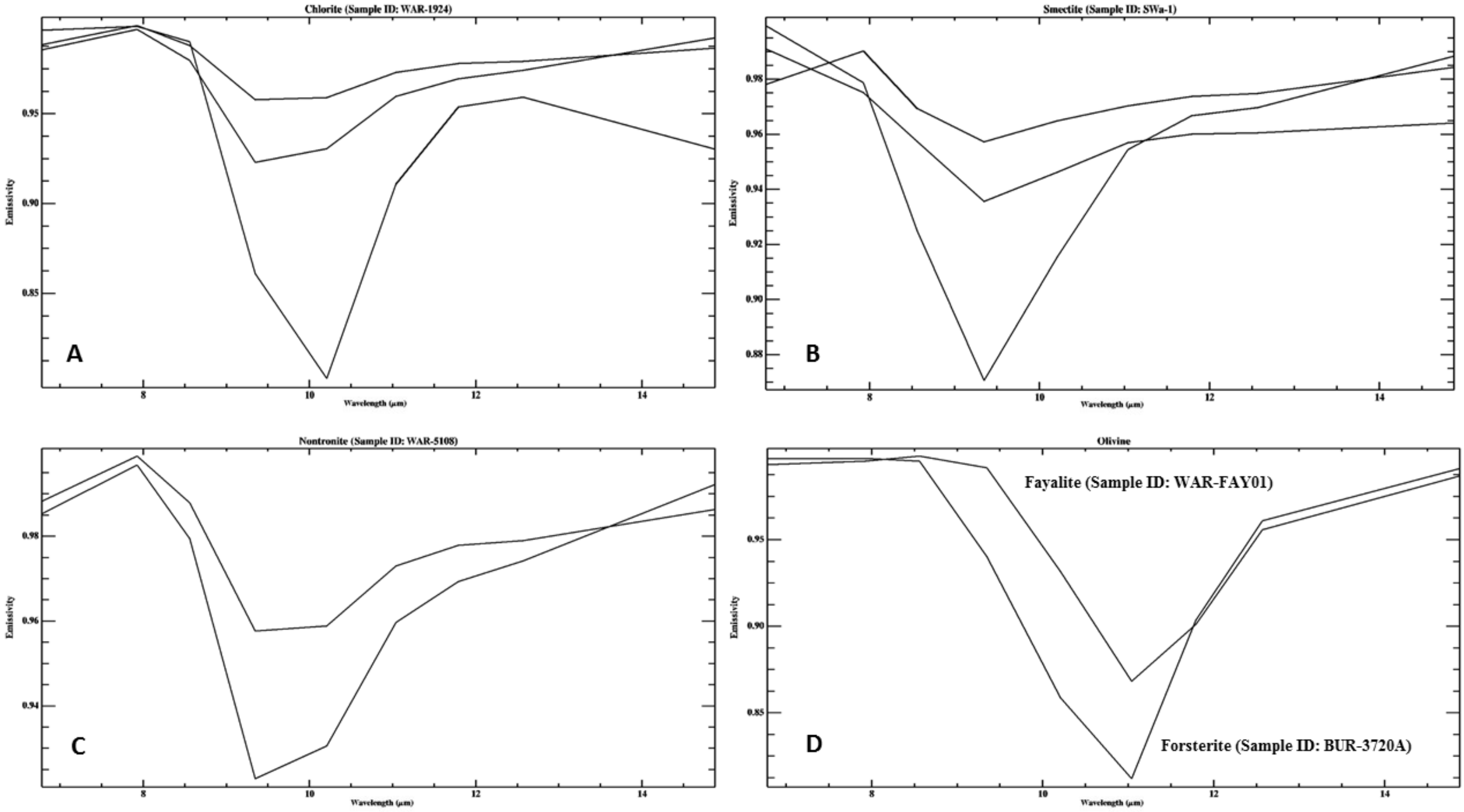

Figure 10: Arizona State University (ASU) TIR spectral library for Fe/Mg phyllosilicates and Olivine (http://speclib.asu.edu/). (A) Three spectra of Chlorite sample WAR-1924 with emissivity low between 9.35 and 10.21 μm; (B) Three spectra of Smectite sample SWa-1 a with an emissivity low at 9.35 μm; (C) Two spectra of Nontronite sample WAR-5108 with emissivity low between 9.35 and 10.21 μm.; and (D) sample spectra for the two major groups of Olivine - Fayalite WAR-FAY01 and Forsterite BUR-3720A, both with emissivity low at 11.04 μm.

3.2 Nili Fossae Crustal Outcrop

3.2.1. Selected Data

A 21 km length crustal outcrop (21.926° N, 77.219° E) within one of the Nili Fossae fractures was selected for spectral comparison with the phyllosilicates in Tyrrhena Terra impact crater. I checked that this selected area is not near complex impact craters with a diameter size of ≥ 7 km to avoid possible exposure to shocked phyllosilicates that might affect the spectral comparison. This study assumes that the crustal outcrop phyllosilicates are less affected by impacts. Two CRISM FRT data are available covering the area with multispectral summary products showing strong presence of phyllosilicates. Only one THEMIS IR data was used because it already covers the whole study area. The chosen THEMIS data has an average surface temperature of 250.08 K and an average atmospheric dust and water opacity of 0.08 which is lower than the maximum limit of 0.15. Table 5 shows the Image ID of the CRISM and THEMIS datasets used.

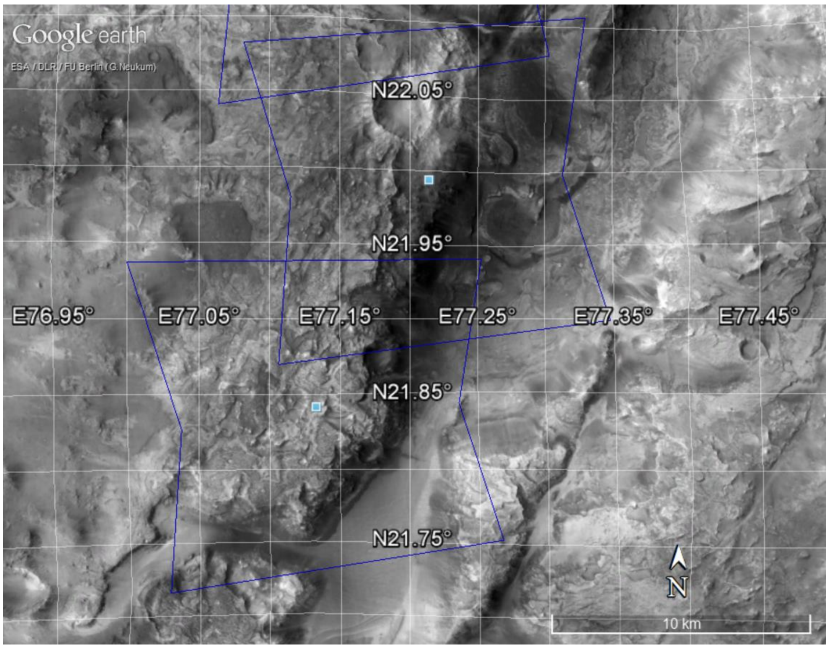

Figure 11: Selected area in Nili Fossae. Blue boxes show CRISM FRT data coverage.

Datasets	Image ID
CRISM FRT	frt0000a4fc_07_if166l_trr3 frt0000871c_07_if166l_trr3
THEMIS Daytime IR	I37499019

Table 5: CRISM and THEMIS datasets used for the Nili Fossae crustal outcrop study.

3.2.2. CRISM NIR Summary Products and Wavelength Maps

The PFM browse product was also used to distinguish Fe/Mg phyllosilicates in the two CRISM FRT images of the crustal outcrop. It revealed distinct patterns in cyan and blue (Fig. 12). Cyan indicates higher values of D2300 and BD2290 summary products than BD2355 and blue indicates higher values of BD2290. These colors, cyan and blue, indicate the presence of Fe/Mg smectites in the area (Viviano-Beck et al., 2014).

Wavelength maps displayed the deepest absorption features occurring between 2.29 and 2.31 μm in green and yellow colors respectively (Fig. 12). This wavelength range supports the result from the PFM summary product where the cyan color indicates the presence of Fe/Mg smectites.

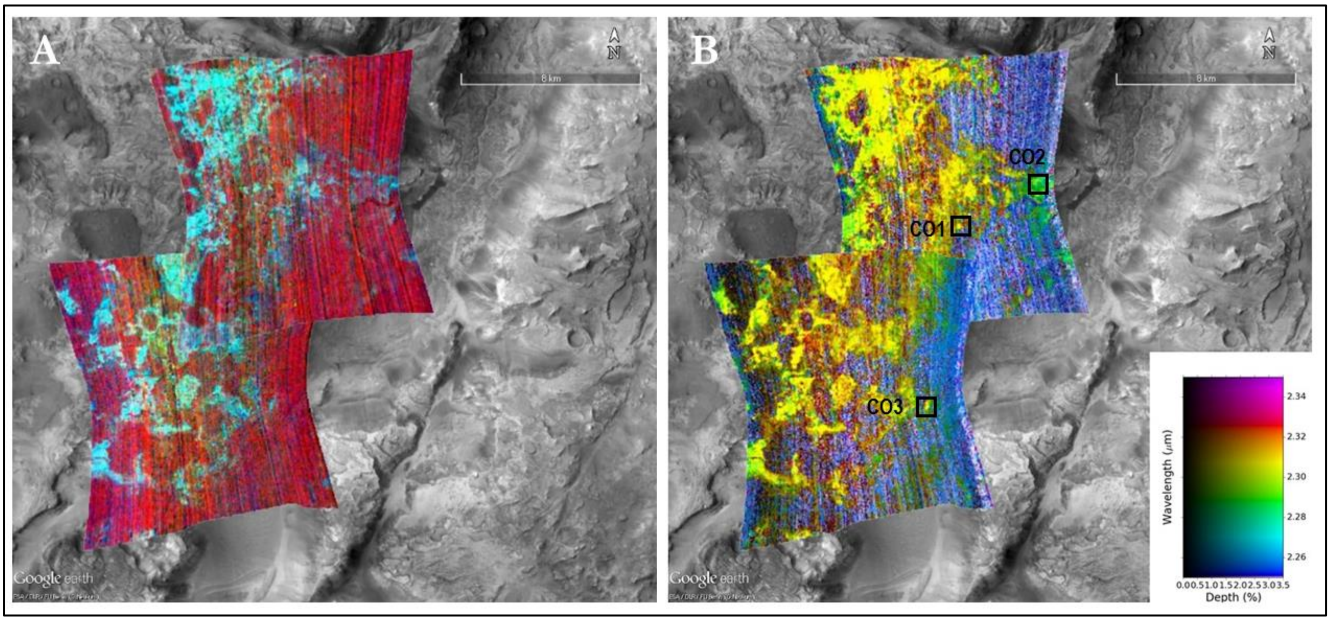

Figure 12: PFM browse products (A) and Wavelength maps (B) for the Nili Fossae crustal outcrop. Average spectra were extracted based on the combined results. CO1 – Crustal Outcrop 1, CO2 – Crustal Outcrop 2, and CO3 – Crustal Outcrop 3

3.2.3. CRISM NIR Spectral Ratio

Three ROIs were chosen that showed distinct spectra in the study area (Fig. 12B). The extracted spectra were averaged and enhanced using the spectral ratio method. The ratioed averaged spectra clearly has diagnostic features of Fe/Mg phyllosilicates with hydration bands in ~1.4 μm (except for Crustal Outcrop 2) and 1.9 μm, and between 2.29 and 2.32 μm due to Fe/Mg-OH bonds (Fig. 13). In comparison with the CRISM spectral library, all spectra resembled Fe/Mg smectite (Fig. 13).

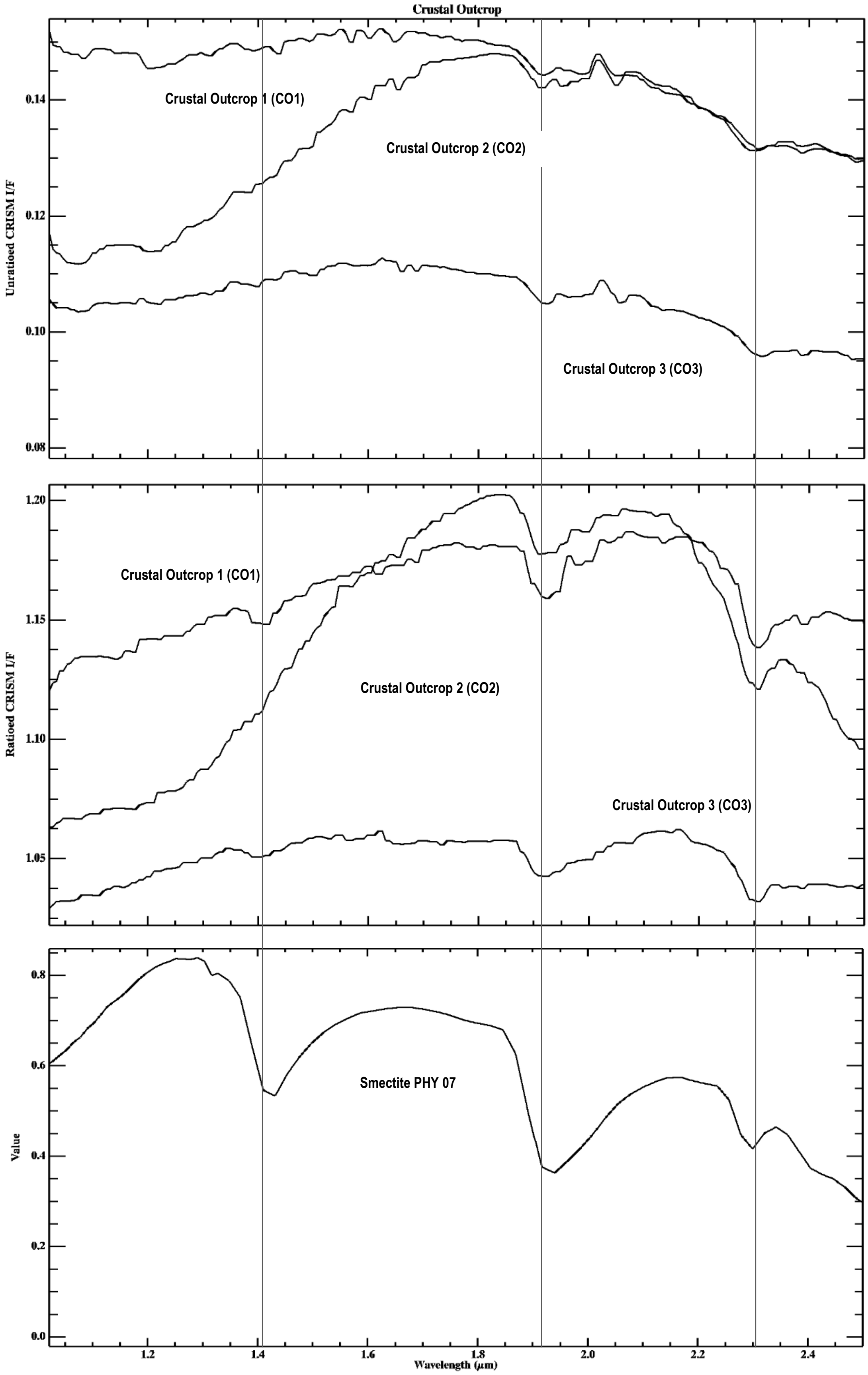

Figure 13: Unratioed and Ratioed average spectra from the crustal outcrop. Gray lines show diagnostic absorption features of Fe/Mg phyllosilicate. CRISM library spectra are shown for comparison.

3.2.4. THEMIS Decorrelation Stretch and Emissivity Spectra

There are four spectrally distinct components in the decorrelation stretched 8-7-5 image – purple, yellow, green, and blue (Fig. 14).

In order to compare SWIR and TIR spectra in phyllosilicate detection, the selected ROIs in the DCS image overlap with the ROIs chosen in the near-infrared data. The average spectrum is then extracted for each ROI (Fig. 14, Table A1).

Crustal Outcrop 1 (CO1) and Crustal Outcrop 2 (CO2) have an emissivity low in bands 5 and 6; whereas Crustal Outcrop 3 (CO3) has an emissivity low in longer wavelengths, between bands 7 and 8 (Fig. 14). Thus, CO1 and CO2 are likely Fe/Mg phyllosilicates while CO3 exhibits a mafic composition such as olivine (Fig. 10). This interpretation is further supported when compared to the TIR spectral library (Fig. 10).

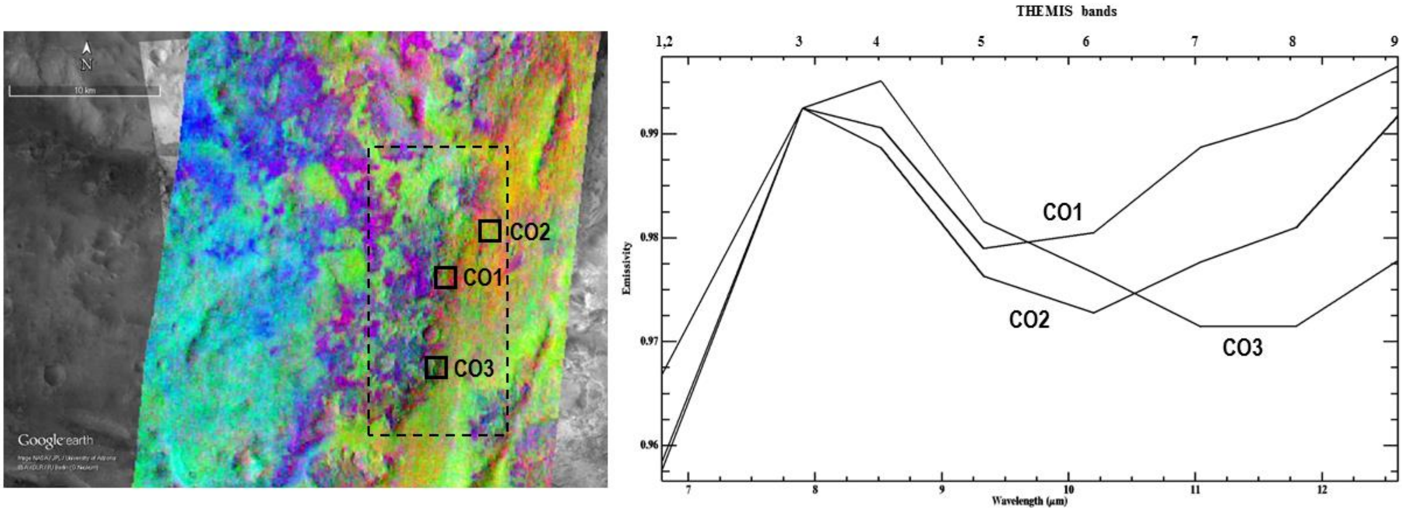

Figure 14: THEMIS DCS 8-7-5 emissivity image of the Nili Fossae crustal outcrop (Left image). Dashed box shows study area coverage. Average emissivity spectra extracted from ROIs in the emissivity image (Right image). CO1 – Crustal Outcrop 1, CO2 – Crust Outcrop 2, and CO3 – Crustal Outcrop 3

This chapter has shown the selected impact crater in the Tyrrhena Terra and the crustal outcrop in the Nili Fossae based on the image availability, coverage, and selection criteria described in section 2.2. Quick assessment and visual analysis of the selected images were performed using summary products and wavelength maps for CRISM data and decorrelation stretched 8-7-5 for THEMIS data. This is to initially check the presence of phyllosilicates in the impact crater and in the crustal outcrop. From this procedure, ROIs were selected to extract representative average spectra of phyllosilicates in each geologic context. Note that since this study aims to look at the SWIR and TIR spectral properties of a shocked phyllosilicate, the selected ROIs should coincide in the two datasets to compare the phyllosilicate detection in two wavelength ranges and in different geologic context.

The following chapter contains the interpretation of results and speculations that aim to answer all the research questions. It will also include comparison of the obtained results to previous studies.

4 DISCUSSION

This study considers shock effects as a possible cause for the spectral discrepancy between the SWIR and TIR in phyllosilicate detection in remotely sensed data, since the Martian surface is heavily bombarded with impact craters. As demonstrated by laboratory impact experiments, impact or shock effects can damage the mineral structure of Fe/Mg phyllosilicate, causing spectral changes which can remain unnoticed in the SWIR, but are apparent in TIR (Friedlander et al., 2015; Gavin et al., 2013). The spectra become amorphous with increasing shock pressure and this can be observed in the TIR region, specifically at 8-12 μm and 16-25 μm. Note that the spectral changes in the mineral structure overlaps with THEMIS's spectral resolution at 8-12 μm. On the other hand, spectral changes due to thermal effects caused by impacts are evident in the SWIR, showing reduced OH and water absorption features at ~1.4 μm and ~1.9 μm (Che & Glotch, 2012, 2014; Friedlander et al., 2015). These laboratory impact experiments provide data with the highest spatial and spectral resolution. Therefore, CRISM and THEMIS datasets, existing Martian datasets with high spatial and spectral resolution, were used for this study.

After I performed various methods to check, extract, and compare the spectra in CRISM SWIR and THEMIS TIR in different geologic contexts, impact/shock effects could have caused the spectral discrepancy. However, there may be other factors aside from impact effects that result to spectral discrepancy in the SWIR and TIR data on Mars. These will be discussed in detail below.

4.1 SWIR and TIR image spectra of phyllosilicates in Nili Fossae Crustal Outcrop

The shortwave-infrared and thermal infrared spectra in the selected area in Nili Fossae agree in the detection of Fe/Mg phyllosilicates. Both spectra show presence of Fe/Mg phyllosilicates.

The extracted SWIR spectra, particularly of CO1 and CO3, show the diagnostic features of an Fe/Mg phyllosilicate at ~1.4 μm, ~1.9 μm, and between 2.30 and 2.35 μm (Bishop et al., 2008). Note that there is a possibility that the ~1.9 μm feature is a remnant of the CO_2 absorption correction at 2.0 μm. But as observed from the spectra, the ~1.9 μm is evident and is exactly located at ~1.9 μm. Therefore, it is considered a water absorption feature rather than an artifact from atmospheric correction. The CO2 spectrum is different from CO1 and CO3 spectra because it lacks the ~1.4 μm feature, but it is still identified as Fe/Mg phyllosilicate (Fig. 13). I suggest that this feature is a result of dehydroxylation, where the depth of the OH band is reduced due to thermal effects from impacts or volcanic events (Che et al., 2011). The Nili Fossae area is covered by impact craters and volcanic flows from Syrtis Major, a shield volcano southwest of Nili Fossae. It is possible that phyllosilicates in the selected area are exposed to such processes. Moreover, although I made sure that the selected area is less covered by impacts, it cannot be ruled out that shocked phyllosilicates are transported in the area due to aeolian or fluvial activity.

In the thermal-infrared spectra, the emissivity lows in CO1 and CO2 occur at 9.33 μm and 10.2 μm and are similar to the emissivity lows in the TIR spectral library of Fe/Mg phyllosilicates. Although the CO2 spectrum lacks the ~1.4 μm feature in the near-infrared, the TIR spectrum further supports that it is still identified as Fe/Mg phyllosilicate. In contrast, the emissivity low in CO3 occurs in longer wavelengths, and so it indicates a presence of mafic mineral such as Olivine rather than Fe/Mg phyllosilicate. The author believes that THEMIS pixels showing presence of Fe/Mg phyllosilicates within the CO3 ROI are very few and is obscured when average spectra was extracted (at least 100 pixels per

ROI for THEMIS data) since there are more THEMIS pixels indicating mafic minerals as shown in DCS 8-7-5 image (Fig.14).

Taken together, the agreement between the SWIR and TIR spectra in Fe/Mg phyllosilicate detection, specifically in CO1 and CO2, supports the assumption that phyllosilicates in this area are less affected by impact processes or are non-shocked phyllosilicates. In the case of the CO3 spectrum, the spectral discrepancy observed between the SWIR and TIR is due to a few THEMIS pixels indicating the presence of Fe/Mg phyllosilicates within the ROI, and not because of impact effects.

4.2 SWIR and TIR image spectra of phyllosilicates in Tyrrhena Terra Impact Crater

The selected unnamed impact crater in Tyrrhena Terra shows an apparent discrepancy between the SWIR and TIR wavelength ranges in the detection of phyllosilicates. However, this discrepancy can have multiple causes.

The PFM summary products/spectral indices show that there is strong abundance of Fe/Mg phyllosilicates inside the crater. However, when compared to wavelength maps, the phyllosilicates appear less abundant. Detailed spectral analysis reveals that there are two spectral signatures present from the spatially distinct patterns shown in the summary products and wavelength maps: (1) a spectrum that has diagnostic absorption features of an Fe/Mg phyllosilicate and (2) a spectrum without these diagnostic features. The former, where all ROIs were extracted, seems to be relatively less abundant in terms of area and resembles chlorite and Fe/Mg smectite, albeit with very subtle ~1.4 μm feature particularly in the ejecta. This reduced depth of the OH band may be attributed to dehydroxylation due to impacts (Che & Glotch, 2012). However, it may also be a diagnostic feature of a chlorite spectrum, since chlorite spectrum in the CRISM spectral library shows a subtle ~1.4 μm feature. Whereas the latter, which is widespread, could indicate dust cover or impact melt (Tornabene et al., 2013). Combining summary products, wavelength maps, and detailed spectral analysis shows that Fe/Mg phyllosilicates are present in the impact crater; however less abundant than what was shown using only summary products.

As a result, the limitations of summary products/spectral indices are possibly one of the causes of the discrepancy between the SWIR and TIR in phyllosilicate detection in remotely sensed data. This study has demonstrated that summary products have overestimated the relative abundance of Fe/Mg phyllosilicates in the impact crater, when in fact, it is less when compared to wavelength maps. Although a summary product captures the spectral feature unique to identify a specific mineralogy, this method doesn't work all the time as observed. As an example, I noticed that the PFM summary product identified a spectrum as possible Fe/Mg phyllosilicate, despite the spectrum not having distinct absorption features between 2.30 – 2.35 μm (see red boxes in Fig. 6).

Thermal infrared spectral analysis gave a different, but complementary perspective on the phyllosilicate detection in the impact crater. ROIs were selected in the DCS 8-7-5 image that coincide with ROIs in the CRISM summary products and wavelength maps identified as Fe/Mg phyllosilicates. This is to check the spectral discrepancy between the SWIR and TIR assumed to be caused by impacts. As observed, the ROI located in the crater peak shows a similar spectral character as the surrounding plains with an emissivity low at 11.04 μm; while the ROIs in the crater floor and ejecta have similar spectral composition with emissivity lows at 9.33 μm and 11.04 μm. This implies that the crater peak does not show the presence of phyllosilicates and possibly is composed of mafic materials; whereas the crater floor and ejecta indicate the presence of phyllosilicates, albeit mixed with mafic materials.

The dissimilarity between the SWIR and TIR spectra in phyllosilicate detection in the crater peak could be caused by shock effects or impact processes. The magnitude of the shock waves from an impact is strongest at the impact point and declines as it radiates outward (French, 1998). Since this study assumes that phyllosilicates in the impact crater were excavated by impact, the spectral discrepancy is possibly caused by intense shock effects altering the mineral structure.

Alternatively, since the crater peak has similar a spectral composition as the surrounding plains as observed from the DCS 8-7-5 image, it may be possible that plain deposits obscured the phyllosilicate detection in TIR. These deposits are possibly brought by winds into the crater, since there are no water features such as gullies that connect the inside of the crater to the plains.

Another reason for the spectral discrepancy is may be due to limited spatial resolution and linear mixing in THEMIS resolution. In CRISM's 18m spatial resolution, Fe/Mg phyllosilicates were identified in the crater peak. However, in THEMIS 100m spatial resolution, it appears that THEMIS cannot resolve the Fe/Mg phyllosilicates detected in CRISM data because these clays are not extensive or abundant enough to be distinguished in a THEMIS pixel. Moreover, linear mixing in a thermal-infrared pixel causes the spectra to appear homogeneous even though it is a mixture of multiple components because the TIR's optical path length is smaller than most grains (Gillespie, 1992; Ramsey & Christensen, 1998). Thus, if the Fe/Mg phyllosilicates are not abundant enough to be resolved in a THEMIS pixel, its spectra can be masked by spectra from more abundant minerals.

In summary, the spectral discrepancy observed between the SWIR and TIR in phyllosilicate detection in the impact crater can be attributed to other factors aside from impact/shock processes. Limitations of summary products/spectral parameters, limited spatial resolution, and spectral mixing of different materials are other possible causes of the apparent spectral discrepancy in remotely sensed data from different sensors. Shocked phyllosilicates are assumed to be present in the impact crater, but because of the aforementioned limitations, it will be difficult to distinguish them.

4.3 Data Quality

In all CRISM data, I noticed that the depth of spectral features are not deeper than noise (see unratioed spectra in Figures 7, 8, and 13). This is the reason why I only chose very few ROIs that represent the spectra of phyllosilicates in the area. The use of the spectral ratio method has possibly reduced the systematic noise in the spectra and enhanced the absorption depth between 2.30 and 2.35 μm. However, if I am not careful in choosing a spectrum for the denominator, I may add unwanted spectral features in the enhanced spectrum, particularly in the shorter wavelengths. This will increase random noise.

The selection of THEMIS data covering the Tyrrhena Terra impact crater was difficult because most images contain very low average surface temperature (< 240 K). High surface temperature (≥ 240K) is significant in order to increase signal-to-noise ratio in an image which makes extracting information easier.

4.4 Comparison of Results to Previous Studies

Some researches rely on summary products/spectral indices to detect presence and relative abundance of Martian phyllosilicates in SWIR and TIR datasets (Bandfield, 2002; McDowell & Hamilton, 2009; Michalski et al., 2010; Rogers & Bandfield, 2009). They have observed an apparent discrepancy between the two wavelength ranges based on these indices. This study has shown that spectral indices can mistakenly identify a spectrum as a certain mineral, when there is no such mineral when careful inspection of the image spectra is performed. This can lead to overestimation of relative abundance of phyllosilicates as what happened in the PFM summary products. When this issue was addressed by carefully inspecting the image spectra, it was observed that relative abundance of phyllosilicates in CRISM images is less and this corresponds with the relative abundance of phyllosilicates observed in THEMIS image. Therefore, issues with summary products/spectral parameters can cause such spectral discrepancy between the SWIR and TIR in the detection of phyllosilicates; and are not necessarily caused by impacts or shock effects.

Based on results from laboratory impact experiments, this study has considered shock effects as possible cause for the spectral discrepancy observed between the SWIR and TIR in the phyllosilicate detection on Mars. However, after performing various techniques to extract and analyse the SWIR and TIR spectra of phyllosilicates in different geologic contexts in CRISM and THEMIS data, it was observed that impact or shock effects may not be the only cause of the spectral discrepancy. The discrepancy may also be caused by issues with the datasets. Thermal effects from impacts, as demonstrated by laboratory impact experiments, could possibly explain the reduced ~1.4 μm feature observed in the extracted SWIR spectra in the ejecta of the Tyrrhena Terra impact crater. However, this subtle ~1.4 μm feature may only show the typical depth of a ~1.4 μm feature in a chlorite spectrum. The spectral detection of shocked phyllosilicates in TIR is found to be difficult due to limited spatial resolution and spectral mixing in a THEMIS pixel. This implies that the spatial and spectral resolution of THEMIS data cannot verify the results from laboratory impact experiments. Moreover, laboratory impact experiments are performed in a controlled environment where external factors such as dusts and mineral mixtures are excluded. Hence, the impact experiment results can only partially explain the role of impacts/shock effects in the spectral discrepancy observed in remotely sensed data; since it does not include influence of dusts and mixtures which are commonly seen in Martian terrains. Given all these issues, it would be difficult to distinguish the spectra of shocked phyllosilicate due to impacted mineral structure on Mars in TIR using the THEMIS data.

4.5 Summary of Findings

This thesis has demonstrated that CRISM and THEMIS data can be combined to detect phyllosilicates despite differences in wavelength range. However, the challenges encountered may involve differences in spatial resolution. For example, in CRISM's 18m spatial resolution, Fe/Mg phyllosilicates were identified in all regions of interest in the Nili Fossae crustal outcrop. However, in THEMIS 100m spatial resolution, it appears that THEMIS cannot resolve the Fe/Mg phyllosilicates detected in one of the ROIs in CRISM data because these clays are not abundant enough to be distinguished in a THEMIS pixel.

To distinguish the spectral properties of phyllosilicates associated with impact craters, a comparison was made between phyllosilicates in a crustal outcrop and an impact crater. This study assumes that phyllosilicates in the impact crater were excavated by impact, causing the spectral discrepancy between the SWIR and TIR in the detection of phyllosilicates. Intense impact or shock effects could damage the mineral structure, thus altering the spectra. However, from visual and spectral analyses of the images, the spectral discrepancy between the SWIR and TIR spectra can be attributed to other factors aside from impact/shock processes. Limitations of summary products/spectral parameters, limited spatial resolution, and spectral mixing of different materials are other possible causes of the apparent spectral discrepancy in remotely sensed data from different sensors. Shocked phyllosilicates are assumed to be present in the impact crater, but because of the aforementioned limitations, it will be difficult to distinguish them.

Thermal effects, as demonstrated by laboratory impact experiments, could possibly explain the reduced ~1.4 μm feature particularly in the CO2 spectrum in the Nili Fossae crustal outcrop. However, the reduced ~1.4 μm feature in all the phyllosilicate spectra in the ejecta of the Tyrrhena Terra impact crater could just be a typical depth of a ~1.4 μm feature in a chlorite spectrum and not caused by impacts. Moreover, laboratory impact experiments are performed in a controlled environment where external factors such as dusts and mineral mixtures are excluded. Hence, the impact experiment results can only partially explain the role of impacts/shock effects in the spectral discrepancy observed in remotely sensed data; since it doesn't include influence of dusts and mixtures which are commonly seen in Martian terrains.

Given all these issues, direct evidence of shocked phyllosilicate spectra in remotely sensed data cannot be obtained using the spatial and spectral resolution of CRISM and THEMIS data.

5 CONCLUSION

Combined and detailed spectral analysis of CRISM SWIR and THEMIS TIR data indicate the presence of Fe/Mg phyllosilicates, both in the Nili Fossae crustal outcrop and in the Tyrrhena Terra impact crater.

Using summary products, wavelength maps, and decorrelation stretched maps, ROIs that reveal Fe/Mg phyllosilicate were selected for spectral comparison between the SWIR and TIR in different geologic context. Fe/Mg phyllosilicates were identified in Nili Fossae crustal outcrop from both wavelength regions. This is expected as it was assumed that phyllosilicates in this area are non-shocked phyllosilicates and are less affected by impact processes. For the Tyrrhena Terra impact crater, Fe/Mg phyllosilicates were also detected, but here a spectral discrepancy between the SWIR and TIR was observed. In this study, reduced ~1.4 μm feature was observed in the SWIR spectra in the ejecta, which is possibly caused by thermal effects from impacts. However, this subtle ~1.4 μm feature could be the typical depth of a ~1.4 μm feature in a chlorite spectrum. The spectral detection of impacted mineral structure are difficult to distinguish in TIR because of issues encountered in THEMIS data. Therefore, the cause of spectral difference between the SWIR and TIR in the detection of Fe/Mg phyllosilicate have another explanations than shock/impact effects. Limitations in the use of spectral parameters/indices, presence of dusts, spectral mixing, and limited spatial and spectral resolution are possible reasons for the spectral discrepancy. Thus, distinguishing shocked phyllosilicate spectra due to damaged mineral structure in remotely sensed data is difficult.

Given the issues encountered, it is difficult to use CRISM and THEMIS data to validate results from the laboratory impact experiments, although it has the highest spatial resolution for thermal-infrared imagery on Mars. Moreover, laboratory experiments are performed in a controlled environment, hence external factors such as dusts and other mineral mixtures common on Martian terrains are not included. Most likely, the results of the laboratory impact experiments won't completely explain the spectral discrepancy observed between the SWIR and TIR spectra of phyllosilicates on Mars.

Overall, direct evidence of the shocked phyllosilicate spectra in remotely sensed data cannot be obtained using the spatial and spectral resolution of the CRISM and THEMIS data. A much higher spatial and spectral resolution imageries or in-situ measurements would be needed in order to validate results from laboratory impact experiments.

.

6 RECOMMENDATIONS

Based on the obtained results, the following are the author's recommendations:

- To combine THEMIS spatial resolution with that of TES hyperspectral resolution. This may increase chances or possibly provide further insights in the spectral detection of shocked phyllosilicates in TIR.

- To test the findings of this study, it is recommended to include more impact craters that meet the selection criteria. Although I mentioned that there is only one impact crater in the Tyrrhena Terra that meets the selection criteria, there's also another one at 13.40° S, 93.70° E. However, it is composed of overlapping impact craters, therefore the phyllosilicates present may not be pre-existing materials excavated from depth, but rather result of post-impact alteration due to multiple impacts. But for the sake of getting more information about the spectral discrepancy due to impacts, I recommend to take a look at this impact crater.

7 APPENDIX

Table A1. Full Image IDs, Locations, and Number of Pixels of the Extracted Average Spectra

Label in Figure	Image ID	Center Pixel	Number of Pixels per ROI *(ROI type: Rectangle)*
Figure 6B			
CP1	frt0001652d_07_if164l_trr3	X:133 Y:440	73
CP2	frt0001652d_07_if164l_trr3	X:253 Y:500	89
CF	frt0001652d_07_if164l_trr3	X:402 Y:547	55
E1	frt00006483_07_if164l_trr3	X:402 Y:230	79
E2	frt00006483_07_if164l_trr3	X:556 Y:258	72
E3	frt00013844_07_if164l_trr3	X:546 Y:322	61
Figure 9			
CP	I17695028	X:397 Y:8382	154
CF	I17695028	X:429 Y:8382	120
E	I17695028	X:455 Y:8584	120
Figure 12B			
CO1	frt0000a4fc_07_if166l_trr3	X:616 Y:326	55
CO2	frt0000a4fc_07_if166l_trr3	X:407 Y:445	69
CO3	frt0000871c_07_if166l_trr3	X:581 Y:380	68
Figure 14			
CO1	I37499019	X:807 Y:2998	110
CO2	I37499019	X:785 Y:3009	90
CO3	I37499019	X:753 Y:3098	108

LIST OF REFERENCES

Amador, E. S., & Bandfield, J. L. (2016). Elevated bulk-silica exposures and evidence for multiple aqueous alteration episodes in Nili Fossae, Mars. *Icarus*, *276*, 39–51. doi:10.1016/j.icarus.2016.04.015

Bakker, W. H. (2013). HypPy Hyperspectral Python Software Package. Retrieved from https://www.itc.nl/personal/bakker/hyppy.html

Bakker, W. H., van Ruitenbeek, F. J. A., van der Werff, H. M. A., Zegers, T. E., Oosthoek, J. H. P., Marsh, S. H., & van der Meer, F. D. (2014). Processing OMEGA/Mars Express hyperspectral imagery from radiance-at-sensor to surface reflectance. *Planetary and Space Science*, *90*, 1–9. doi:10.1016/j.pss.2013.11.007

Baldridge, A. M., Lane, M. D., & Edwards, C. S. (2013). Searching at the right time of day: Evidence for aqueous minerals in Columbus crater with TES and THEMIS data. *Journal of Geophysical Research E: Planets*, *118*(2), 179–189. doi:10.1029/2012JE004225

Bandfield, J. L. (2002). Global mineral distributions on Mars. *Journal of Geophysical Research*, *107*(E6), 5042. doi:10.1029/2001JE001510

Bandfield, J. L., Rogers, D., Smith, M. D., & Christensen, P. R. (2004). Atmospheric correction and surface spectral unit mapping using thermal emission imaging system data. *Journal of Geophysical Research E: Planets*, *109*(10), 1–17. doi:10.1029/2004JE002289

Barnhart, C. J., & Nimmo, F. (2011). Role of impact excavation in distributing clays over Noachian surfaces. *Journal of Geophysical Research*, *116*(E1), E01009. doi:10.1029/2010JE003629

Bibring, J.-P., Langevin, Y., Gendrin, A., Gondet, B., Poulet, F., Berthé, M., … Drossart, P. (2005). Mars surface diversity as revealed by the OMEGA/Mars Express observations. *Science (New York, N.Y.)*, *307*(5715), 1576–1581. doi:10.1126/science.1108806

Bishop, J. L., Lane, M. D., Dyar, M. D., & Brown, a. J. (2008). Reflectance and emission spectroscopy study of four groups of phyllosilicates: smectites, kaolinite-serpentines, chlorites and micas. *Clay Minerals*, *43*(1), 35–54. doi:10.1180/claymin.2008.043.1.03

Carter, J., Poulet, F., Bibring, J.-P., Mangold, N., & Murchie, S. (2013). Hydrous minerals on Mars as seen by the CRISM and OMEGA imaging spectrometers: Updated global view. *Journal of Geophysical Research: Planets*, *118*(4), 831–858. doi:10.1029/2012JE004145

Che, C., & Glotch, T. D. (2012). The effect of high temperatures on the mid-to-far-infrared emission and near-infrared reflectance spectra of phyllosilicates and natural zeolites: Implications for martian exploration. *Icarus*, *218*(1), 585–601. doi:10.1016/j.icarus.2012.01.005

Che, C., & Glotch, T. D. (2014). Thermal alteration: A possible reason for the inconsistency between OMEGA/CRISM and TES detections of phyllosilicates on Mars? *Geophysical Research Letters*, *41*(2), 321–327. doi:10.1002/2013GL058649

Che, C., Glotch, T. D., Bish, D. L., Michalski, J. R., & Xu, W. (2011). Spectroscopic study of the dehydration and/or dehydroxylation of phyllosilicate and zeolite minerals. *Journal of Geophysical Research*, *116*(E5), E05007. doi:10.1029/2010JE003740

Christensen, P. R., Engle, E., Answar, S., Dickenshied, S., Noss, D., Gorelick, N., Weiss-Malik, M. (2009). JMARS - A Planetary GIS. In *American Geophysical Union, Fall Meeting*. Retrieved from http://adsabs.harvard.edu/abs/2009AGUFMIN22A..06C

Christensen, P. R., Bandfield, J. L., Hamilton, V. E., Ruff, S. W., Kieffer, H. H., Titus, T. N., … Greenfield, M. (2001). Mars Global Surveyor Thermal Emission Spectrometer experiment: Investigation description and surface science results. *Journal of Geophysical Research: Planets*, *106*(E10), 23823–23871. doi:10.1029/2000JE001370

Christensen, P. R., Jakosky, B. M., Kieffer, H. H., Malin, M. C., McSween, Jr., H. Y., Nealson, K., … Ravine, M. (2004). The Thermal Emission Imaging System (THEMIS) for the Mars 2001 Odyssey Mission. *Space Science Reviews*, *110*(1/2), 85–130. doi:10.1023/B:SPAC.0000021008.16305.94

Ehlmann, B. L., Mustard, J. F., Murchie, S. L., Bibring, J.-P., Meunier, A., Fraeman, A. a, & Langevin, Y. (2011). Subsurface water and clay mineral formation during the early history of Mars. *Nature*, *479*(7371), 53–60. doi:10.1038/nature10582

Ehlmann, B. L., Mustard, J. F., Swayze, G. a., Clark, R. N., Bishop, J. L., Poulet, F., … Murchie, S. L. (2009). Identification of hydrated silicate minerals on Mars using MRO-CRISM: Geologic context near Nili Fossae and implications for aqueous alteration. *Journal of Geophysical Research*, *114*, E00D08. doi:10.1029/2009JE003339

Fairén, A. G., Chevrier, V., Abramov, O., Marzo, G. a, Gavin, P., Davila, A. F., … McKay, C. P. (2010). Noachian and more recent phyllosilicates in impact craters on Mars. *Proceedings of the National Academy of Sciences of the United States of America*, *107*(27), 12095–12100. doi:10.1073/pnas.1002889107

French, B. M. (1998). *Traces of Catastrophe: A Handbook of Shock-Metamorphic Effects in Terrestrial Meteorite Impact Structures*. Houston.

Friedlander, L. R., Glotch, T. D., Bish, D. L., Dyar, M. D., Sharp, T. G., Sklute, E. C., & Michalski, J. R. (2015). Structural and spectroscopic changes to natural nontronite induced by experimental impacts between 10 and 40 GPa. *Journal of Geophysical Research: Planets*, *120*(5), 888–912. doi:10.1002/2014JE004638

Gavin, P., Chevrier, V., Ninagawa, K., Gucsik, a., & Hasegawa, S. (2013). Experimental investigation into the effects of meteoritic impacts on the spectral properties of phyllosilicates on Mars. *Journal of Geophysical Research E: Planets*, *118*(1), 65–80. doi:10.1029/2012JE004185

Gillespie, A. R. (1986). Lithologic Mapping of Silicate Rocks using TIMS. In *The TIMS Data User's Workshop* (pp. 29–44). JPL.

Gillespie, A. R. (1992). Spectral mixture analysis of multispectral thermal infrared images. *Remote Sensing of Environment*, *42*(2), 137–145. doi:10.1016/0034-4257(92)90097-4

Gillespie, A. R., Kahle, A. B., & Walker, R. E. (1986). Color enhancement of highly correlated images. I. Decorrelation and HSI contrast stretches. *Remote Sensing of Environment*, *20*(3), 209–235. doi:10.1016/0034-4257(86)90044-1

Hazen, R. M., Sverjensky, D. a., Azzolini, D., Bish, D. L., Elmore, S. C., Hinnov, L., & Milliken, R. E. (2013). Clay mineral evolution. *American Mineralogist*, *98*(11-12), 2007–2029. doi:10.2138/am.2013.4425

Loizeau, D., Carter, J., Bouley, S., Mangold, N., Poulet, F., Bibring, J. P., … Murchie, S. L. (2012). Characterization of hydrated silicate-bearing outcrops in Tyrrhena Terra, Mars: Implications to the alteration history of Mars. *Icarus*, *219*(1), 476–497. doi:10.1016/j.icarus.2012.03.017

Martin, P. E., & Barker, E. F. (1932). The Infrared Absorption Spectrum of Carbon Dioxide. *Physical Review*, *41*(3), 291–303. doi:10.1103/PhysRev.41.291

McDowell, M. L., & Hamilton, V. E. (2009). Seeking phyllosilicates in thermal infrared data: A laboratory and Martian data case study. *Journal of Geophysical Research*, *114*(E6), E06007. doi:10.1029/2008JE003317

McGuire, P. C., Bishop, J. L., Brown, A. J., Fraeman, A. A., Marzo, G. A., Frank Morgan, M., … Wolff, M. J. (2009). An improvement to the volcano-scan algorithm for atmospheric correction of CRISM and OMEGA spectral data. *Planetary and Space Science*, *57*(7), 809–815. doi:10.1016/j.pss.2009.03.007

Meunier, A. (2005). *Clays* (1st ed.). Springer-Verlag Berlin Heidelberg. doi:10.1007/b138672

Michalski, J., Poulet, F., Bibring, J. P., & Mangold, N. (2010). Analysis of phyllosilicate deposits in the Nili Fossae region of Mars: Comparison of TES and OMEGA data. *Icarus*, *206*(1), 269–289. doi:10.1016/j.icarus.2009.09.006

Milliken, R. E., Mustard, J. F., Poulet, F., Jouglet, D., Bibring, J.-P., Gondet, B., & Langevin, Y. (2007). Hydration state of the Martian surface as seen by Mars Express OMEGA: 2. H 2 O content of the surface. *Journal of Geophysical Research*, *112*(E8), E08S07. doi:10.1029/2006JE002853

Morgan, F., Seelos, F., & Murchie, S. (2009). CRISM Data Users' Workshop CAT Tutorial. In *MRO/CRISM Data Users' Workshop*. Retrieved from http://pds-geosciences.wustl.edu/missions/mro/CRISM_Workshop_090322_CAT_MFM.pdf

Murchie, S., Arvidson, R., Bedini, P., Beisser, K., Bibring, J.-P., Bishop, J., … Wolff, M. (2007). Compact Reconnaissance Imaging Spectrometer for Mars (CRISM) on Mars Reconnaissance Orbiter (MRO). *Journal of Geophysical Research*, *112*(E5), E05S03. doi:10.1029/2006JE002682

Murray, K. C., Christensen, P. R., Mehall, G. L., & Gorelick, N. S. (2012). *Thermal Emission Imaging System 2001 Mars Odyssey: THEMIS Geometric Processing User's Guide*. Retrieved from http://static.mars.asu.edu/pds/ODTGEO_v1/geometry/geometry.pdf

Mustard, J. F., Murchie, S. L., Pelkey, S. M., Ehlmann, B. L., Milliken, R. E., Grant, J. A., … Wolff, M. (2008). Hydrated silicate minerals on Mars observed by the Mars Reconnaissance Orbiter CRISM instrument. *Nature*, *454*(7202), 305–309. doi:10.1038/nature07097

Owen, T., Biemann, K., Rushneck, D. R., Biller, J. E., Howarth, D. W., & Lafleur, A. L. (1977). The composition of the atmosphere at the surface of Mars. *Journal of Geophysical Research*, *82*(28), 4635–4639. doi:10.1029/JS082i028p04635

Parente, M. (2008). A New Approach to Denoising CRISM Images. In *Lunar and Planetary Science XXXIX*. Retrieved from http://www.lpi.usra.edu/meetings/lpsc2008/pdf/2528.pdf

Pelkey, S. M., Mustard, J. F., Murchie, S., Clancy, R. T., Wolff, M., Smith, M., … Gondet, B. (2007). CRISM multispectral summary products: Parameterizing mineral diversity on Mars from reflectance. *Journal of Geophysical Research E: Planets*, *112*(8), 1–18. doi:10.1029/2006JE002831

Piatek, J.L., Moersch, J. E. (2006). A Strategy for Atmospheric correction of THEMIS Infrared Data. In *Lunar and Planetary Science XXXVII*. Retrieved from http://www.lpi.usra.edu/meetings/lpsc2006/pdf/1158.pdf

Ramsey, M. S., & Christensen, P. R. (1998). Mineral abundance determination: Quantitative deconvolution of thermal emission spectra. *Journal of Geophysical Research: Solid Earth*, *103*(B1), 577–596. doi:10.1029/97JB02784

Rogers, A. D., & Bandfield, J. L. (2009). Mineralogical characterization of Mars Science Laboratory candidate landing sites from THEMIS and TES data. *Icarus*, *203*(2), 437–453. doi:10.1016/j.icarus.2009.04.020

Salisbury, J. W., & Walter, L. S. (1989). Thermal infrared (2.5–13.5 μm) spectroscopic remote sensing of igneous rock types on particulate planetary surfaces. *Journal of Geophysical Research*, *94*(B7), 9192. doi:10.1029/JB094iB07p09192

Tornabene, L. L., Moersch, J. E., McSween, H. Y., Hamilton, V. E., Piatek, J. L., & Christensen, P. R. (2008). Surface and crater-exposed lithologic units of the Isidis Basin as mapped by coanalysis of THEMIS and TES derived data products. *Journal of Geophysical Research*, *113*(E10), E10001. doi:10.1029/2007JE002988

Tornabene, L. L., Osinski, G. R., McEwen, A. S., Wray, J. J., Craig, M. a., Sapers, H. M., & Christensen, P. R. (2013). An impact origin for hydrated silicates on Mars: A synthesis. *Journal of Geophysical Research E: Planets*, *118*(5), 994–1012. doi:10.1002/jgre.20082

van Ruitenbeek, F. J. a., Bakker, W. H., van der Werff, H. M. a., Zegers, T. E., Oosthoek, J. H. P., Omer, Z. a., … van der Meer, F. D. (2014). Mapping the wavelength position of deepest absorption features to explore mineral diversity in hyperspectral images. *Planetary and Space Science*, *101*, 108–117. doi:10.1016/j.pss.2014.06.009

Vivian-Beck, C. E., Seelos, F. P., Murchie, S. L., Kahn, E. G., Seelos, K. D., Taylor, H. W., … Morgan, F. M. MRO CRISM Type Spectral Library, NASA Planetary Data System (2015). Retrieved from http://crismtypespectra.rsl.wustl.edu/

Viviano, C. E., & Moersch, J. E. (2012). A technique for mapping Fe/Mg-rich phyllosilicates on Mars using THEMIS multispectral thermal infrared images. *Journal of Geophysical Research*, *117*(E7), E07007. doi:10.1029/2011JE003985

Viviano, C. E., & Moersch, J. E. (2013). Using THEMIS data to resolve the discrepancy between CRISM/OMEGA and TES modeled phyllosilicate abundance in Mawrth Vallis. *Icarus*, *226*(1), 497–509. doi:10.1016/j.icarus.2013.06.005

Viviano-Beck, C. E., Seelos, F. P., Murchie, S. L., Kahn, E. G., Seelos, K. D., Taylor, H. W., … Morgan, M. F. (2014). Revised CRISM spectral parameters and summary products based on the currently detected mineral diversity on Mars. *Journal of Geophysical Research: Planets*, *119*(6), 1403–1431. doi:10.1002/2014JE004627